



Progressive forest canopy water loss during the 2012–2015 California drought

Gregory P. Asner¹, Philip G. Brodrick, Christopher B. Anderson, Nicholas Vaughn, David E. Knapp, and Roberta E. Martin

Department of Global Ecology, Carnegie Institution for Science, Stanford, CA 94305

Contributed by Gregory P. Asner, November 30, 2015 (sent for review November 10, 2015); reviewed by Craig D. Allen and Robert Green

The 2012–2015 drought has left California with severely reduced snowpack, soil moisture, ground water, and reservoir stocks, but the impact of this estimated millennial-scale event on forest health is unknown. We used airborne laser-guided spectroscopy and satellite-based models to assess losses in canopy water content of California's forests between 2011 and 2015. Approximately 10.6 million ha of forest containing up to 888 million large trees experienced measurable loss in canopy water content during this drought period. Severe canopy water losses of greater than 30% occurred over 1 million ha, affecting up to 58 million large trees. Our measurements exclude forests affected by fire between 2011 and 2015. If drought conditions continue or reoccur, even with temporary reprieves such as El Niño, we predict substantial future forest change.

canopy water | climate change | drought | forest health | imaging spectroscopy

California has undergone progressive drought since 2012, with the cumulative rainfall deficit in 2015 described as a one in a 1,000-y event (1). As a result, concern has grown over the ecological and societal effects of the drought throughout the environmental conservation, management, and resource policy communities (2). Such concerns are likely to increase as rising temperatures interact with droughts in California and around the world (3–5).

Forests of California are of particular interest because they include the tallest, most massive, and oldest trees on Earth, as well as provide a wide variety of goods and services to the state of California and the world. These services include habitat for numerous plant and animal species, carbon storage for climate change mitigation, water provisioning for a myriad of industries and communities, timber for wood products, and ecotourism (6). Combined with high air temperatures and insect infestations, the 2012–2015 drought has generated a large pulse of tree mortality in California (7). This event may have cascading effects on forest fire susceptibility and severity, animal habitat and biological diversity, water resources, and carbon sequestration. However, tree mortality mapping provides a limited understanding of forest vulnerability and adaptation, because the observations do not directly resolve forest physiological responses to ongoing changes in climate. To improve predictions of how forests will change in the future, spatially and temporally continuous measurements of canopy functional responses to climate change are needed.

Monitoring forest canopy physiology in the context of drought and other climate perturbations has proven challenging, because the onset and progression of canopy stress is not easily revealed in traditional satellite observations (8). Newer technologies, such as high-fidelity imaging spectroscopy (HiFIS), may help to break this barrier (9, 10). HiFIS measures the spectral radiance reflected from the land surface in narrow, overlapping, and contiguous spectral channels (11). After compensation for illumination and atmospheric effects, HiFIS-measured spectral reflectance yields quantitative measurements of the mass-concentration of biologically important molecules and elements (12–15), some of which are diagnostic and predictive of vegetation responses to climate change.

One of the most operational HiFIS measurements is canopy water content (CWC), which is the total amount of liquid water

in the foliage of a canopy. CWC is an indicator of tree physiological status because it underpins important plant functions, including light interception and growth (16–18). It is broadly correlated with leaf water potential during times of water stress (19–21), and thus has served as an indicator of progressive drought effects on forest canopies (8). CWC is also a useful predictor for vegetation flammability (22). CWC can be estimated from HiFIS in units of water volume (e.g., liters) in the canopy on a per area (e.g., square meter) basis, derived from the depth and shape of 118 spectral absorption features centered at 980 nm and 1,160 nm (23, 24). By combining HiFIS measurements with 3D forest imaging via light detection and ranging (LiDAR) scanning, it is possible to exclude nonforest canopies, such as grasses and short shrubs, as well as bare ground, rock cover, and infrastructure, from the intended measurement (25). This data-fusion technique, called laser-guided HiFIS, allows for the measurement and projection of forest CWC in three dimensions.

HiFIS and LiDAR technologies are not currently available from satellites. The Carnegie Airborne Observatory (CAO) is one of the few systems that can make laser-guided HiFIS measurements on an operational basis (26). Nonetheless, the time needed to cover a large area, such as the ~13.4 million ha of forest in California, requires additional techniques that combine aircraft measurements with an integrated suite of statewide geospatial data (27, 28). We combined airborne laser-guided HiFIS, multivariate satellite and environmental data, and geostatistical modeling to develop high-resolution forest CWC maps of California (*SI Appendix*, Figs. S1–S4 and Table S1).

The airborne and satellite measurements were collected in August 2015, allowing for the derivation of geostatistically robust

Significance

The state of California has a globally important economy and a population exceeding 38 million. The state relies on its forested watersheds to support numerous services, such as water provisioning, carbon storage, timber products, ecotourism, and recreation. However, secular changes in air temperature, combined with periodic and prolonged drought, pose a compounding challenge to forest health. Here we use new remote-sensing and modeling techniques to assess changes in the canopy water content of California's forests from 2011 to 2015. Our resulting maps of progressive canopy water stress identify at-risk forest landscapes and watersheds at fine resolution, and offer geographically explicit information to support innovative forest management and policies in preparation for climate change.

Author contributions: G.P.A. designed research; G.P.A., P.G.B., C.B.A., N.V., D.E.K., and R.E.M. performed research; G.P.A., P.G.B., C.B.A., N.V., D.E.K., and R.E.M. analyzed data; and G.P.A., P.G.B., and R.E.M. wrote the paper.

Reviewers: C.D.A., US Geological Survey; and R.G., Jet Propulsion Laboratory.

The authors declare no conflict of interest.

Freely available online through the PNAS open access option.

¹To whom correspondence should be addressed. Email: gpa@carnegiescience.edu.

This article contains supporting information online at www.pnas.org/lookup/suppl/doi:10.1073/pnas.1523397113/-DCSupplemental.

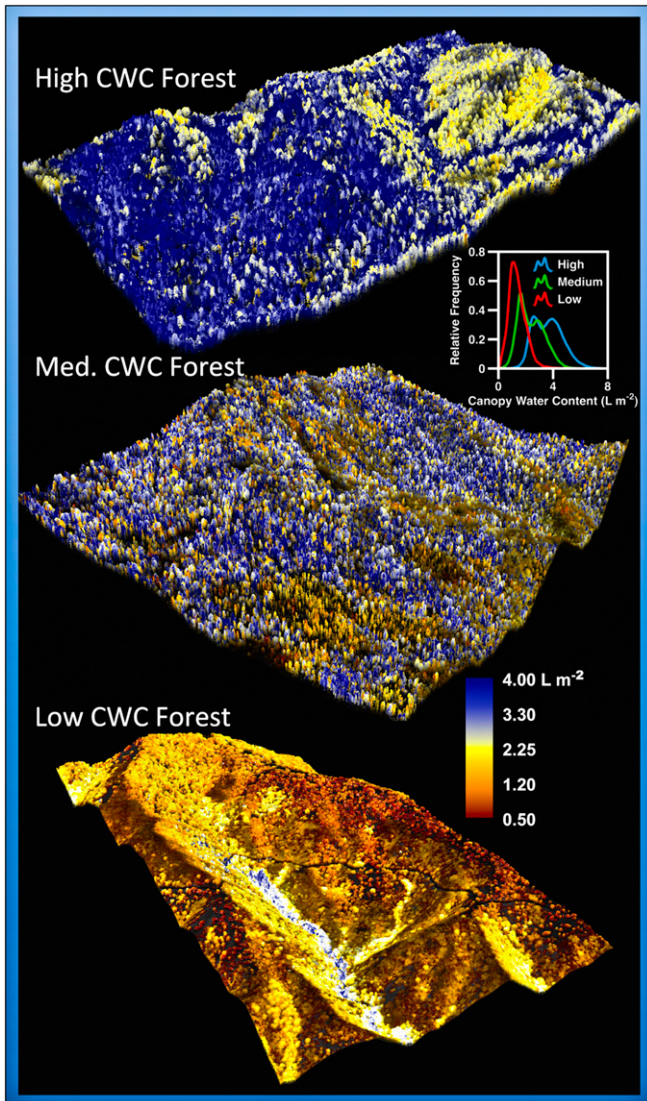


Fig. 1. Example CAO images of forest 3D canopy water content (CWC) highlighting landscapes of about 1,000 ha each, with high, medium, and low CWC. (Inset) Graph shows the frequency distribution of CWC in liters of water per square meter (L/m^2). These landscape examples were taken from Muir Woods National Monument (high CWC), Sequoia-Kings Canyon National Park (medium CWC), and Los Padres National Forest (low CWC). Field and airborne observations, as well as US Forest Service studies (7), indicate massive mortality in the low CWC landscape shown.

relationships between HiFIS and satellite data using a deep learning model (*SI Appendix*). These relationships were used to scale up the 2015 HiFIS measurements to the entire forested region of California. In addition, statewide multivariate satellite data were compiled for 2011, 2013, and 2014, and used to retrospectively estimate forest CWC and change from 2011 to 2015 using our modeling technique. The goal was to quantify CWC changes over 4 years as a means to understand forest canopy physiological responses to progressive drought.

Results and Discussion

Forest Canopy Water Content in 2015. Twelve days of flight operations yielded 1.8 million ha of direct airborne CWC estimates at 2-m spatial resolution. Three example landscapes totaling ~3,000 ha are shown in Fig. 1. As depicted in these images, CWC in each landscape strongly varied based on tree species and condition, local

topography, and other factors. Across California, we observed enormous CWC variability in the aircraft imagery, with patterns linked to forest type and geographic location throughout the state. Some landscapes were comprised of individual trees with CWC that was greatly suppressed relative to neighboring vegetation. Other landscapes showed widespread suppression of CWC, with spatial patterns following the terrain. These results indicated that the upscaling and modeling of the CWC measurements to statewide maps needed to be accomplished at relatively fine spatial resolution. We selected 30-m \times 30-m resolution (0.09 ha) as the resolution for modeling all forests of California (*SI Appendix*).

Ten percent of the original aircraft CWC data were left out of the scaling step to validate the statewide 2015 model. These validation data were selected randomly from aircraft coverage acquired throughout the state, and were comprised of 1.2 million measurements. Regression analyses showed an R^2 of 0.82 and root mean squared error of 0.45 L/m^2 of forest canopy (*SI Appendix*, Fig. S5). Mean absolute deviation was 0.33 L/m^2 . These results indicated that the statewide model captures the spatial and ecological patterns of CWC measured using airborne laser-guided HiFIS.

We assessed the importance of environmental factors mediating the patterns of forest CWC as measured by the aircraft sensors (*SI Appendix*). Geographic location and elevation accounted for a large proportion of the measured variation in CWC (*SI Appendix*, Fig. S6). Beyond these factors, a suite of satellite vegetation metrics was important in modeling forest CWC. These metrics included the fractional cover of green leaf photosynthetic vegetation, bare ground exposure, and shortwave-infrared reflectance, the latter being sensitive to canopy water content (29, 30). This suite of satellite-based vegetation measurements were critically important for scaling up the direct CWC observations from airborne laser-guided HiFIS, and for developing retrospective models of change in CWC.

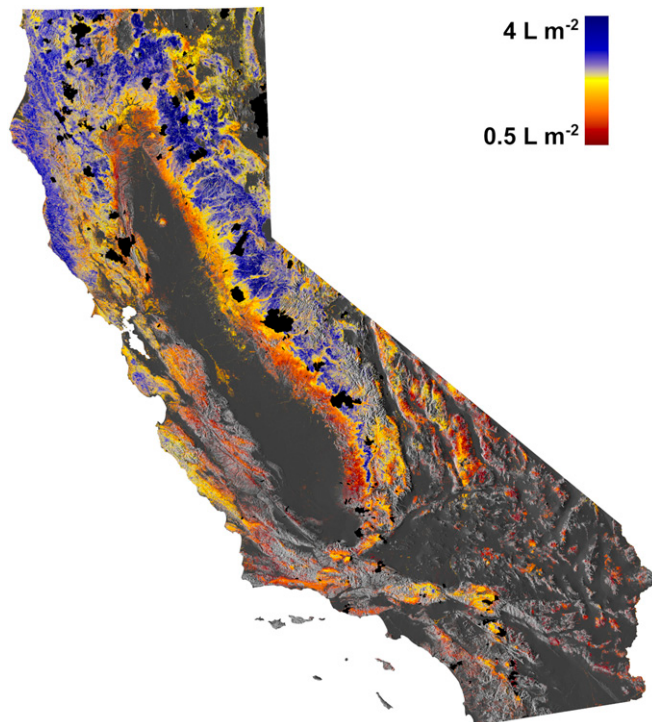


Fig. 2. Forest canopy water content (CWC) reported in liters per square meter for the state of California as of August 2015. Black areas indicate fire extents between 2011 and 2015 by the US Forest Service (31).

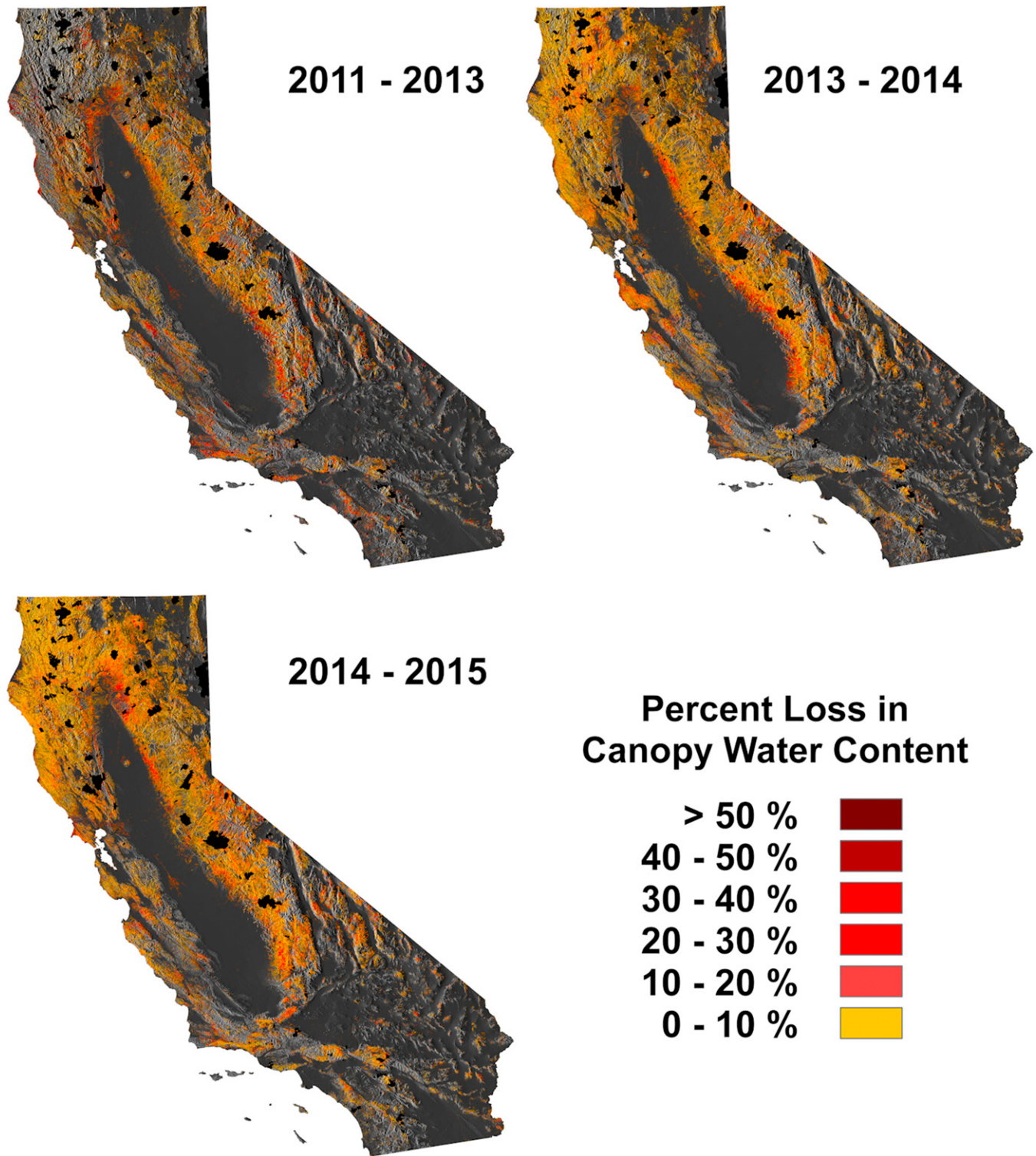


Fig. 3. Forest canopy water loss from 2011 to 2013, 2013 to 2014, and 2014 to 2015. Black areas indicate fire extents reported between 2011 and 2015 by the US Forest Service (31).

The statewide model for August 2015 indicated local- to regional-scale gradients in forest canopy water content (Fig. 2 and *SI Appendix*, Figs. S7–S9). The lowest modeled CWC values ($<1.0 \text{ L/m}^2$) were observed in southern Californian forests as well as in lower elevation forests encircling the Central Valley. This included lower elevations of the Sierra Nevada Mountains. Additional low-CWC forests were modeled on slopes above forested

drainages and river valleys, as well as in extensive swaths throughout much of the state's wildland-urban interface.

Forest Canopy Change 2011–2015. Statewide retrospective analyses revealed major changes in forest CWC between 2011 and 2015 (Fig. 3). We emphasize the importance of drought in the following results, but note that changes in CWC integrate the effects

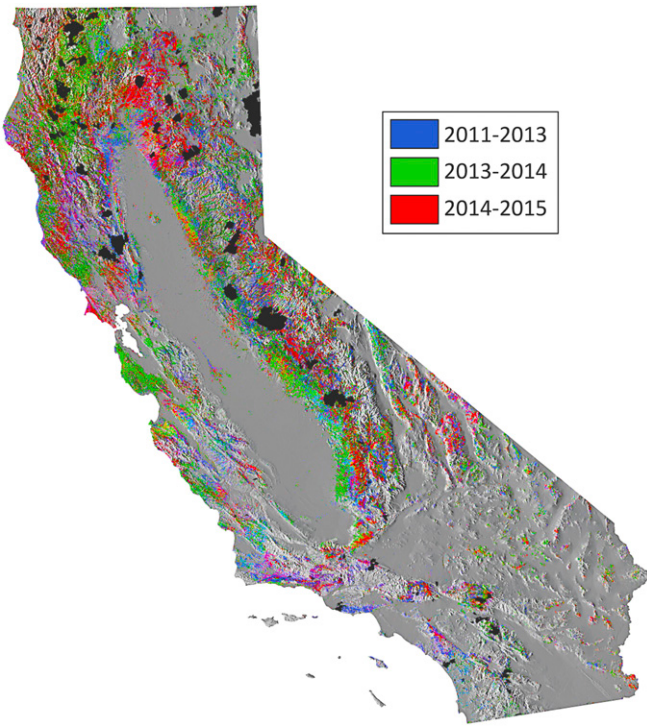


Fig. 4. The geography of forest canopy water loss from 2011 to 2015, partitioned spatially by onset period of observation. Only water losses of at least 5% are displayed. Black areas indicate fire extents reported between 2011 and 2015 by the US Forest Service (31).

of drought, widespread insect damage, and high temperatures (3, 31). Our results exclude all reported burned areas mapped between 2011 and 2015 by the US Forest Service (31), so as not to conflate CWC loss caused by fire damage. We also generated a map showing the period in which CWC decreased by at least 5% (Fig. 4 and *SI Appendix*, Figs. S10–S12). This map reveals the spatially progressive nature of forest canopy response to drought through time.

Results indicated that the area of forest negatively impacted in the 2011–2013, 2013–2014, and 2014–2015 periods was 4.0, 6.1, and 6.6 million ha, respectively (Figs. 3 and 4 and *SI Appendix*, Fig. 5A). From 2011 to 2013, many of the lower-elevation forests and woodlands encircling California’s Central Valley underwent CWC losses (Fig. 4, blue). By 2014, additional water loss was found in lowland and foothill forest settings, such as the Santa Cruz Mountains (Fig. 4, green). By 2015, much more extensive drought-related forest canopy water loss was observed at higher elevation, well above the zones of initial water loss (Fig. 4, red).

To place the CWC results in the context of potentially at-risk trees, we mapped stem densities provided in 5,565 US Forest Service Forest Inventory and Analysis (FIA) field plots (32) to estimate the maximum number of “large” trees (≥ 12.7 cm diameter at breast height) affected by drought-related factors (*SI Appendix*, Figs. S13 and S14). From 2011 to 2013, the forested area of 4.0 million ha contained up to 283 million large trees that showed a measurable degree of water loss (Fig. 5B). In the 2013–2014 interval, 6.1 million ha of forest with up to 507 million large trees were measurably affected by drought-related factors. In the 2014–2015 interval, 6.6 million ha and up to 565 million large trees were negatively affected. Although we emphasize that these statistics do not represent mortality, they do point to rapid increases in the vulnerability of millions of trees that were physically and physiologically affected by drought and related factors.

We combined the multiyear results from Fig. 3 into a single map of progressive canopy water stress indicating the cumulative water loss for forests in California, as the sum of percent water losses from 2011 to 2015 (Fig. 6 and *SI Appendix*, Figs. S15–S17). Based on this map, we estimate that 10.6 million ha and up to 888 million large trees underwent progressive, directional decreases in CWC between 2011 and 2015. Of this amount, a total forest area of 5.4 million ha, comprising up to 412 million large trees, decreased in canopy water content by at least 10%. Losses of greater than 30% CWC, a threshold we view as severe based on aircraft videography and visual observations, covered a cumulative area of 1 million ha comprised of up to 58 million large trees.

Although it is conceptually straightforward to link canopy water loss to suppressed growth or carbon uptake in forests (8), it is more challenging to convert maps of CWC loss to estimates of tree mortality. For example, the range of potential mortality responses at 10% CWC loss on a hectare scale is as follows: a 10% decrease in average CWC could represent mortality of up to 8 trees per hectare at FIA’s median California forest stand density of 80 large trees per hectare. On the other hand, 10% CWC loss could be spread among all trees in a hectare, thereby representing a measurable, but likely nonlethal, amount of water loss or leaf area reduction among all trees. However, very few regions selected for airborne CWC mapping showed such evenness in canopy water content by 2015 (Fig. 1). Moreover, analysis of aircraft-based CWC in 2015 against the retrospective, progressive water stress map (Fig. 6) indicated that water losses were strongly associated with tree-scale changes in water content (*SI Appendix*, Table S3). Based on these observations and analyses, we believe that CWC decreases of more than 10% on a hectare basis represent, at a minimum, a major suppression of productivity and reductions in canopy leaf area, and more likely indicate a loss of multiple trees per hectare.

We further interpreted the progressive water loss results based on the US Geological Survey LANDFIRE land-cover classification (*SI Appendix*). From 2011 to 2015, vegetation types showing large declines in CWC (>15%) included lowland mixed conifer-oak, particularly pine-dominated areas, chaparral woodlands, as well as trees in shrubland ecosystems (*SI Appendix*, Table S2). Note again that our minimum canopy height cut-off was 2 m, including in areas classified as shrubland. Major CWC decreases were observed in forests comprised of coastal redwoods in the lowlands, and at higher elevations pinyon-juniper, lodgepole pine,

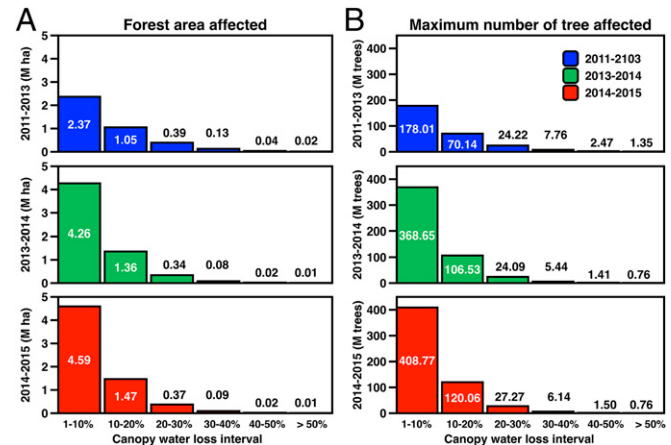


Fig. 5. (A) Mapped forest areas of decreases in canopy water content between 2011–2013, 2013–2014, and 2014–2015. (B) Estimated maximum number of trees (≥ 12.7 cm or 5 inches diameter at breast height) affected for each observation interval.

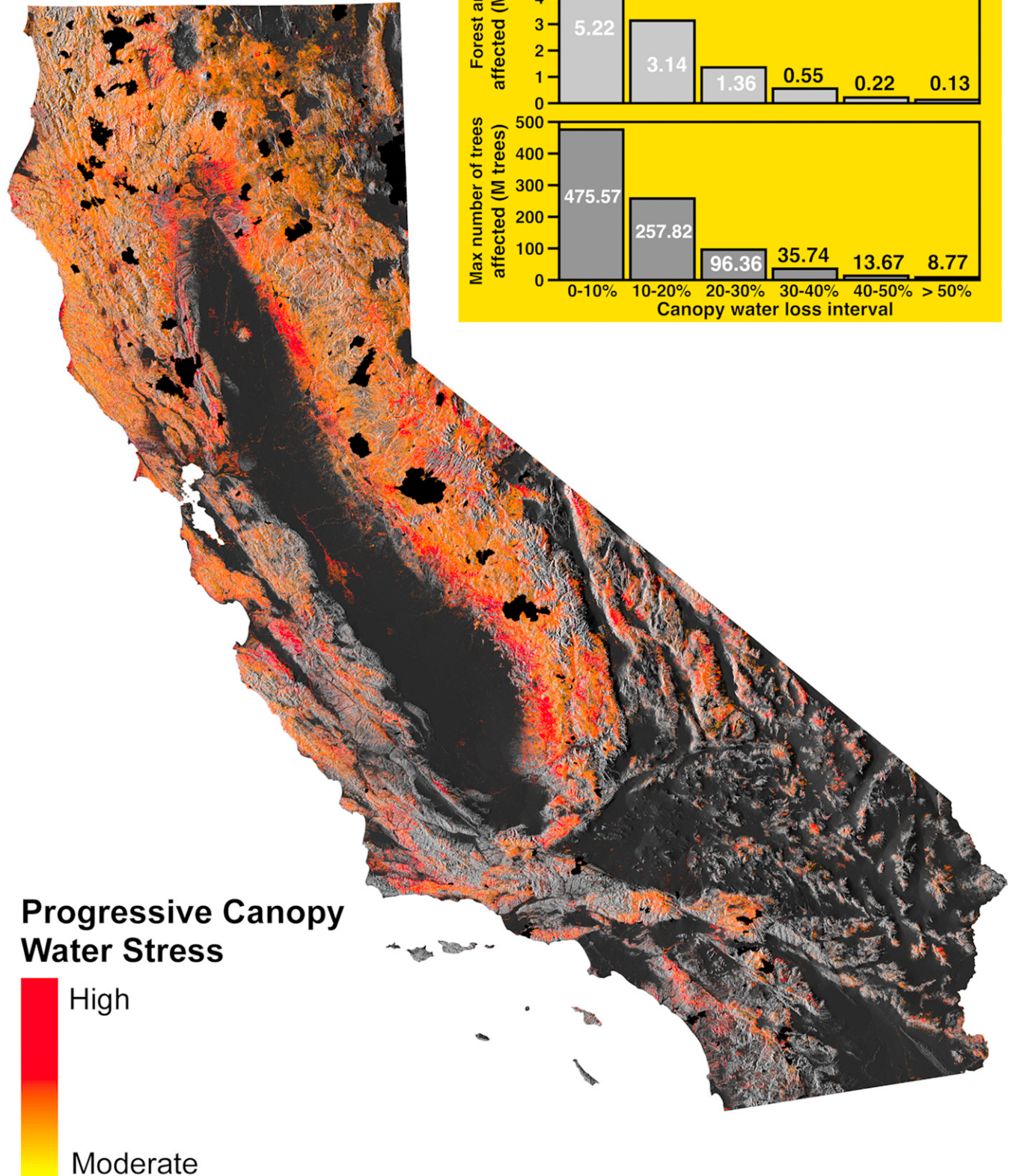


Fig. 6. Progressive forest canopy water stress for the years 2011–2015, computed as the total percentage CWC loss for the study period. Inset graph indicates the mapped forest area and estimated maximum number of trees (≥ 12.7 cm or 5 inches diameter at breast height) affected in differing CWC loss classes. Black areas indicate fire extents reported between 2011 and 2015 by the US Forest Service (31).

red fir, and black oak forests underwent widespread water losses. Only the highest-elevation forests and patches of lower-elevation forests and woodland types showed less (but still measurable) losses in CWC.

Forest Monitoring in a Changing Climate. To our knowledge, our results are the first to reveal progressive forest canopy water loss resulting in highly suppressed canopy water content in many regions of California. By August 2015, much of the state had undergone a measurable decrease in forest CWC since 2011. Over approximately the same time period, low-altitude visual mapping studies conducted by the US Forest Service estimated that roughly 27 million trees died in California forests (7, 33, 34). Major differences in mapping approach preclude a direct comparison of our method to aerial tree counts: Aerial surveys of brown and leafless trees suggest increasing mortality rates over time, whereas our modeled changes in canopy water content serve more of a prognostic role in terms of potential mortality. Nonetheless, map-to-map comparisons indicate a similar overall geographic pattern of canopy water loss (Fig. 6) and mortality (7, 33).

Importantly, our measurements reveal far higher levels of drought-affected forest than can be assessed using visual mapping approaches. We found massive areas of progressive canopy water stress that are geographically aligned with a growing population of observed dead trees. Moreover, if drought continues or reoccurs, there exists a pool of trees spread over millions of hectares of forest that may undergo sufficient CWC loss to result in death. Based on rates of CWC change observed during the drought (Fig. 5), this pool could increase into the hundreds of millions of trees.

Given the wide variety of forest and woodland environments found throughout California, and their variable CWC losses during the 2012–2015 drought, repeated airborne and satellite surveys will be needed to assess longer-term impacts. By combining CWC monitoring with field inventory, it should be possible to develop a capability to predict mortality. Until then, our approach uniquely identifies trees and landscapes of changing vulnerability as climate conditions evolve over time.

CWC monitoring yields spatially explicit information to support innovations in forest conservation, management and resource policy development at multiple scales. The options vary depending upon the scale-dependent technological steps developed and presented here. High-resolution, aircraft-based CWC measurements provide new data on millions of hectares of forest and generate detail on a tree-by-tree basis (Fig. 1). Potential applications of HiFIS data include implementation of prescribed

fire, firebreaks, and other fire-management approaches, hazardous tree removal, ecological corridor and habitat management, and watershed management. At the broad state level, the 30-m resolution models reveal the full extent and depth of impact of drought on California's entire forest canopy. The findings strongly suggest that if drought continues, even with a potential temporary reprieve via a 2015–2016 El Niño (35), we can expect continuing forest change at the regional scale. Long-term resource policy and decision-making efforts may consider such impacts on forest resources, such as by assessing geographically explicit increases in carbon emissions where tree mortality occurs, versus increases in carbon sequestration following tree species migration (e.g., higher elevations). Planning for corridors of species migration in California, such as by expanding protected areas and limiting infrastructural development, is one example strategic use of the new information derived from imaging spectroscopy.

In the context of forest management and resource decision-making, current mainstream satellite technologies provide information only on forest cover, deforestation, and other physical disturbances to forest canopies (36). We currently lack a mission to place a high-fidelity imaging spectrometer into Earth orbit. Such a device will deliver continuous measurements of vegetation canopy water content, along with several other Earth surface chemicals (22, 37). The NASA HypsIRI imaging spectrometer remains in a premission phase of study (11), yet it lacks a clear plan or schedule for deployment. Such a mission could greatly enhance our ability to measure, monitor, and map changes in biospheric composition and function in the face of climate change.

Methods

To assess the effect of progressive drought on California forests, HiFIS and LiDAR data were collected using the Carnegie Airborne Observatory (26). The CAO sensor package includes a dual-laser waveform LiDAR system and a HiFIS that measures in the 380- to 2,510-nm wavelength range (*SI Appendix*). The CAO is able to collect up to 6 ha/s of data during flight. Even at this rapid rate it is unrealistic to provide wall-to-wall coverage of California's ~13.4 million ha of forest. Moreover, even complete coverage would provide only an instantaneous view in time of CWC. Instead, our approach builds upon established methods for using noncontinuous airborne data to train a portfolio of geographically contiguous data to generate statewide geographic models of forest CWC (*SI Appendix*).

ACKNOWLEDGMENTS. This study was supported by the David and Lucile Packard Foundation. The Carnegie Airborne Observatory is currently supported by the Avatar Alliance Foundation, John D. and Catherine T. MacArthur Foundation, Mary Anne Nyburg Baker and G. Leonard Baker Jr., and William R. Hearst III.

- Robeson SM (2015) Revisiting the recent California drought as an extreme value. *Geophys Res Lett* 42(16):6771–6779.
- Brown EG (2015) *State of California Proclamation of a State of Emergency* (Executive Department, State of California, Sacramento, CA).
- Williams AP, et al. (2015) Contribution of anthropogenic warming to California drought during 2012–2014. *Geophys Res Lett*, 42(16):6819–6828.
- Diffenbaugh NS, Swain DL, Touma D (2015) Anthropogenic warming has increased drought risk in California. *Proc Natl Acad Sci USA* 112(13):3931–3936.
- Allen CD, et al. (2010) A global overview of drought and heat-induced tree mortality reveals emerging climate change risks for forests. *For Ecol Manage* 259(4):660–684.
- Chornesky EA, et al. (2015) Adapting California's ecosystems to a changing climate. *Bioscience* 65(3):247–262.
- USFS (2015) *2015 Forest Health Protection Aerial Detection Survey*. Available at www.fs.usda.gov/detail/5/forest-grasslandhealth/. Accessed November 1, 2015.
- Asner GP, Nepstad D, Cardinot G, Ray D (2004) Drought stress and carbon uptake in an Amazon forest measured with spaceborne imaging spectroscopy. *Proc Natl Acad Sci USA* 101(16):6039–6044.
- Shugart HH, et al. (2015) Computer and remote-sensing infrastructure to enhance large-scale testing of individual-based forest models. *Front Ecol Environ* 13(9):503–511.
- Schimel DS, Asner GP, Moorcroft PR (2013) Observing changing ecological diversity in the Anthropocene. *Front Ecol Environ* 11(3):129–137.
- Lee CM, et al. (2015) An introduction to the NASA Hyperspectral InfraRed Imager (HypSIRI) mission and preparatory activities. *Remote Sens Environ* 167:6–19.
- Curran PJ (1989) Remote sensing of foliar chemistry. *Remote Sens Environ* 30:271–278.
- Asner GP, Martin RE, Anderson CB, Knapp DE (2015) Quantifying forest canopy traits: Imaging spectroscopy versus field survey. *Remote Sens Environ* 158(0):15–27.
- Serbin SP, Singh A, McNeil BE, Kingdom CC, Townsend PA (2014) Spectroscopic determination of leaf morphological and biochemical traits for northern temperate and boreal tree species. *Ecol Appl* 24(7):1651–1669.
- Clark RN, et al. (2003) Imaging spectroscopy: Earth and planetary remote sensing with the USGS Tetracorder and expert systems. *J Geophys Res Planets* 108(5131):1–44.
- Chaves MM, et al. (2002) How plants cope with water stress in the field. Photosynthesis and growth. *Ann Bot (Lond)* 89(Spec No):907–916.
- Metcalfe DB, et al. (2008) The effects of water availability on root growth and morphology in an Amazon rainforest. *Plant Soil* 311(1–2):189–199.
- Farooq M, Wahid A, Kobayashi N, Fujita D, Basra SMA (2009) Plant drought stress: Effects, mechanisms and management. *Sustainable Agriculture*, eds Lichthouse E, Navarrete M, Debaeke P, Souchere V, Alberola C (Springer, The Netherlands), pp 153–188.
- Meir P, et al. (2009) The effects of drought on Amazonian rain forests. *Amazonia and Global Change, Geophysical Monograph Series*, eds Keller M, Bustamante M, Gash J, Silva Dias P (American Geophysical Union, Washington, DC), Vol 186, pp 429–449.
- Nepstad DC, et al. (2002) The effects of partial throughfall exclusion on canopy processes, aboveground production, and biogeochemistry of an Amazon forest. *J Geophys Res* 107(D20):1–18.
- Vourlitis GL, et al. (2008) Energy balance and canopy conductance of a tropical semi-deciduous forest of the southern Amazon Basin. *Water Resour Res* 44(3):W03412.
- Ustin SL, Roberts DA, Gamon JA, Asner GP, Green RO (2004) Using imaging spectroscopy to study ecosystem processes and properties. *Bioscience* 54(6):523–534.

23. Gao B-C, Goetz AFH (1990) Column atmospheric water vapor and vegetation liquid water retrievals from airborne imaging spectrometer data. *J Geophys Res* 95(D4): 3549–3564.
24. Green RO, Painter TH, Roberts DA, Dozier J (2006) Measuring the expressed abundance of the three phases of water with an imaging spectrometer over melting snow. *Water Resour Res* 42(10):W10402.
25. Asner GP, et al. (2007) Carnegie Airborne Observatory: In-flight fusion of hyperspectral imaging and waveform light detection and ranging for three-dimensional studies of ecosystems. *J Appl Remote Sens* 1:013536.
26. Asner GP, et al. (2012) Carnegie Airborne Observatory-2: Increasing science data dimensionality via high-fidelity multi-sensor fusion. *Remote Sens Environ* 124(0): 454–465.
27. Mascaro J, et al. (2014) A tale of two “forests”: Random forest machine learning AIDS tropical forest carbon mapping. *PLoS One* 9(1):e85993.
28. Asner GP (2009) Tropical forest carbon assessment: Integrating satellite and airborne mapping approaches. *Environ Res Lett* 4(3):034009.
29. Ustin S, et al. (1996) Estimating canopy water content of chaparral shrubs using optical methods. *Summaries of the Sixth Annual JPL Airborne Earth Science Workshop*, ed Green RO (NASA Jet Propulsion Laboratory, Pasadena, CA), pp 235–238.
30. Ceccato P, Flasse S, Tarantola S, Jacquemoud S, Gregoire JM (2001) Detecting vegetation leaf water content using reflectance in the optical domain. *Remote Sens Environ* 77(1):22–33.
31. USDA (2015) *US Forest Service Fire Detection Maps*. Available at activefiremaps.fs.fed.us/. Accessed November 1, 2015.
32. USDA (2008) *Forest Inventory and Analysis Program*. Available at www.fia.fs.fed.us/. Accessed November 1, 2015.
33. USFS (2015) *1014 Aerial Survey Results: California*. Available at www.fs.usda.gov/detail/r5/forest-grasslandhealth. Accessed November 1, 2015.
34. USFS (2013) *2012 Aerial Survey Results: California*. Available at www.fs.usda.gov/detail/r5/forest-grasslandhealth. Accessed November 1, 2015.
35. NOAA (2015) *El Niño/Southern Oscillation (ENSO) Diagnostic Discussion* (National Weather Service, College Park, MD).
36. GOFC-GOLD (2008) *Reducing Greenhouse Gas Emissions from Deforestation and Degradation in Developing Countries: A Sourcebook of Methods and Procedures for Monitoring, Measuring and Reporting* (Office of GOFC-GOLD Program, Alberta, Canada).
37. Kokaly RF, Asner GP, Ollinger SV, Martin ME, Wessman CA (2009) Characterizing canopy biochemistry from imaging spectroscopy and its application to ecosystem studies. *Remote Sens Environ* 113(0):S78–S91.

Supporting Information

Progressive Forest Canopy Water Loss During the 2012-2015 California Drought

Gregory P. Asner, Philip G. Brodrick, Christopher Anderson,
Nicholas Vaughn, David E. Knapp, Roberta E. Martin

Department of Global Ecology
Carnegie Institution for Science
260 Panama Street
Stanford, CA 94305

(gpa@carnegiescience.edu; pbrodrick@carnegiescience.edu; cbanders@carnegiescience.edu;
nvaughn@carnegiescience.edu; dknapp@carnegiescience.edu; rmartin@carnegiescience.edu)

This file includes:

Methods
References
Figs. S1-S17
Tables S1-S3

Methods

Approach

To assess the effect of progressive drought on California forests, high-fidelity imaging spectroscopy (HiFIS) and Light Detection and Ranging (LiDAR) data were collected using the Carnegie Airborne Observatory (CAO) Airborne Taxonomic Mapping System (AToMS), which is carried onboard a Dornier 228 aircraft (1). The AToMS sensor package includes a dual-laser waveform LiDAR scanner and a HiFIS that measures in the 380-2510 nm wavelength range.

The CAO is able to collect up to 6 ha per second of data during flight, far outpacing any ground-based method for forest assessment. Even at this rate it is unrealistic to provide wall-to-wall coverage of California's ~13.4 million hectares of forest. Moreover, even complete coverage of the state would provide only an instantaneous view in time of canopy water content (CWC). Instead, our approach builds upon established methods for using non-continuous airborne data to train spatially contiguous, satellite-derived data sets to generate statewide geographic models of forest CWC. The modeling method is based on a high-resolution approach originally designed for forest carbon assessment (2), which was developed through testing and analysis in a wide variety of countries and ecosystems (3-7). This method combines readily available satellite and geographic information system datasets at fine spatial resolution with airborne HiFIS and LiDAR data in a modeling framework to develop large-scale, spatially contiguous maps. Here we modified the approach for mapping forest CWC.

Airborne Sampling

The mapping region covers the forests of the State of California. We used the CAO to massively sample plant canopy structure and CWC throughout the portions of California containing woody vegetation. Airborne data sampling was carried out using a grid of 25 x 25 km cells overlain on a vegetation stratification map of California. For flight planning purposes, we used data from the CALVEG geospatial database available from the US Forest Service (<http://www.fs.usda.gov/>). The R5 CALVEG classification system conforms to the National Vegetation Classification Standard. We selected the Ecological Units subsection vegetation layer, containing 193 unique vegetation classes throughout California (**Fig. S1a**). We also stratified the State using 250 m elevation bands from 0 to 1500 m and > 1500 m above sea level (**Fig. S1b**). The intersected CALVEG and elevation data represent a large range of local community information. By systematically sampling across these stratified regions within each grid cell, we ensure that we captured the community variation that exists along the forested areas of the Coast, Sierra Nevada, Cascade, Klamath, and Transverse Ranges. The stratification map contained 1,337 unique vegetation classes within the forested areas of the State, totaling 13,410,879 ha (**Fig. S1c**). While this likely provided over-stratification of geographic variation in canopy structure and CWC at the State level, we used this map to plan flights that ensure maximum sampling density in as many unique regions as possible. We did not survey any grid cells with less than 10% of their area covered by forest.

A total of 1,787,133 ha of airborne data were collected throughout the State (**Fig. S2a**). Of this mapped area, 847,516 ha were collected over forests, totaling 6.32% of the forested area of California. More than half the forested area in State was sampled with a density of 5% or more (shown in green and white

tiles in **Fig. S2b**). Airborne data in the forested regions of northwestern California were sparsely (< 5%) sampled due to extensive fires in August 2015, which restricted airspace due to fire fighting operations and zero visibility flight conditions due to smoke (shown in red, orange and yellow tiles in **Fig. S2b**).

Light Detection and Ranging

Airborne data collection was performed at an altitude of 2000 m above ground level (a.g.l.), an average flight speed of 150 knots, and a mapping swath of 1200 m. Operational settings for the LiDAR were 34° field of view, a pulse repetition frequency of 50 kHz per laser, and a beam divergence of 0.56 mrad (1/e) per laser, resulting in 1-m horizontal resolution data when rasterized with at least four laser shots per m². Laser ranges from the LiDAR were combined with embedded Global Positioning System-Inertial Measurement Unit (GPS-IMU) data and a smoothed best-estimate of trajectory (SBET) to determine the 3-D locations of laser returns, producing a ‘cloud’ of LiDAR data. These points were used to interpolate a raster digital terrain model (DTM) for the ground surface of each landscape. This was achieved using a 10 m x 10 m kernel passed over each flight block, with the lowest elevation estimate in each kernel assumed to be ground. Subsequent points were evaluated by fitting a horizontal plane to each of the ground seed points. If the closest unclassified point is < 5.5° and < 1.5 m higher in elevation, it was classified as ground. The digital surface model (DSM) was created based on interpolations of all first-return points. Measurement of the vertical difference between the DTM and DSM yields a digital canopy model (DCM) of vegetation height above ground.

Imaging Spectroscopy

The CAO Visible-to-Shortwave Infrared (VSWIR) imaging spectrometer measures spectral radiance in 427 channels spanning the 380-2510 nm wavelength range in 5 nm increments with nominally 6-nm spectral response function (full-width at half-maximum). Additional detector rows are used to monitor the instrument dark signal levels.

The VSWIR has a 34° full field-of-view and an instantaneous field-of-view of 1 mrad per imaging element. At 2000 m above ground level (a.g.l.), the VSWIR data collection provided 2-m ground sampling distance, or pixel size, throughout each flight. The VSWIR data were radiometrically corrected from raw DN values to radiance ($\text{mW cm}^{-2} \text{ nm}^{-1} \text{ sr}^{-1}$) using a flat-field correction, radiometric calibration coefficients and spectral calibration data collected in the laboratory. Assessment of measurements over known well characterized surface calibration targets show the VSWIR radiometric calibration agrees within 4% of independent MODTRAN predictions of the incident upwelling radiance.

The standardized GPS pulse-per-second (PPS) measurement recorded within the VSWIR data was used to precisely co-locate the spectral imagery to the LiDAR data. A camera model, created in the laboratory and refined for the flight installation, was used to determine the three-dimensional location and field-of-view of each sensor element, which was combined with the standardized timing information for data co-registration of the data sources. The geometry data from the data fusion were used to atmospherically correct the radiance imagery using a modified version of the ACORN-5 model (Imspec LLC, Glendale, CA USA). To improve aerosol corrections in ACORN-5, the model was iteratively run with different visibilities until the reflectance at 420 nm (which is relatively constant for vegetated pixels) is less than

1% (8). Reflectance imagery was corrected for cross-track brightness gradients using a bidirectional reflectance distribution function (BRDF) modeling approach (8).

One of the most reliable measurements from HiFIS is canopy water content (CWC). CWC is the total amount of liquid water in the foliage of the canopy, and is strongly expressed in the 980 nm and 1160 nm absorption features of canopy spectral reflectance data (Fig. S3). The ACORN-5 software derives surface reflectance using a MODTRAN look-up table and performs an iterative feature fitting to de-correlate atmospheric water vapor and liquid water on the surface, deriving CWC. The CWC metric represents the volume (liters) of water in the foliar canopy on a per-area basis often in units of L m⁻² (9-13).

To ensure the comparability of CWC over the entire State of California, and among flight days, the spectral data used to quantify CWC were filtered/masked using a data-fusion approach capitalizing on the collection and inter-calibration of the boresight-aligned HiFIS and LiDAR observations (14). A tree crown mask was derived from the LiDAR data using a ray tracing model that precisely identifies canopy locations in unobstructed view of the VSWIR imaging spectrometer, and removes spectral pixels that are fully or partially shaded by adjacent foliage, branches or crowns (15). The LiDAR data were also used to mask out (ignore) any vegetation less than 2 m in height.

Statewide Mapping

A supervised machine-learning algorithm was used to scale up the aircraft-based CWC imagery to the full State level. The spatially explicit datasets (**Fig. S4a-o**) used in this study were: (a) fractional cover of photosynthetic vegetation (PV), non-photosynthetic vegetation (NPV) and bare substrate (%), (b) elevation (m a.s.l.), (c-d) topographic slope and aspect (degrees), (e-h) four periods of solar insolation (kWh m⁻²), (i) distance to water bodies such as streams (m), (j and k) Landsat 8 surface reflectance in the shortwave infrared regions (SWIR) from 1.57-1.65 and 2.11-2.29 μm, (l) road density (fraction of road per unit area), relative elevation (m), (n) distance to roads (km), and (o) time since last fire (yr). Map coordinates (UTM 10N) were also included as an input. These input datasets covered the entire State of California, and were co-aligned and if necessary resampled to a 30 m pixel size for standardized use in the modeling. A listing of these input statewide data sets and their sources is provided in **Table S1**.

Each mapped variable provides unique information to the modeling process, and the use of machine-learning algorithms allows us to find nonlinear correlations in high dimensions that may not be apparent to the human eye. Map coordinate data explicitly integrate spatial coordinates into the model. Previous studies have demonstrated that spatial context plays a major role in determining how well machine learning methods scale from local sampling schema to full coverage (6, 16).

Landsat satellite data at 30 m resolution were used to calculate the fractional cover of surface components of photosynthetic vegetation (PV), non-photosynthetic vegetation (NVP), and bare substrate across the State of California. Landsat images at sensor-radiance from days between June 1-August 15 for the years 2011, 2013, 2014 and 2015 were utilized. Imagery from 2012 was excluded because of the gap in contiguous coverage between Landsat 5 and Landsat 8. Selected radiance images were analyzed

using a cloud-ranking algorithm to determine the most cloud and cloud shade-free pixel within the selected timeframe. Following this step, the filtered data were processed using the Carnegie Landsat and Analysis System (CLASlite) (17) to calculate surface reflectance and fractional cover data. The Landsat SWIR-1 and SWIR-2 (abbreviated from shortwave-infrared) channels measure in the 1.57-1.65 μm and 2.11-2.29 μm regions, respectively, by the Landsat 8 satellite (data years 2013-2015). The wavelength designations are slightly different in the Landsat 5 satellite (1.55-1.75 and 2.08-2.35 μm , respectively) used for the 2011 data; however, these minor deviations in the longer wavelengths do not influence the near infrared (NIR) regions where canopy water is active in the spectrum. The SWIR reflectance bands were included because they are known to be sensitive to canopy chemical variations related to water content (9, 10, 13). The fractional cover parameters on the other hand, particularly PV, define canopy green foliar cover, which increases with water content (18-20). These five Landsat-based measurements play a major role in capturing variation in vegetation water content as trained by airborne CWC measurements.

The airborne CWC derived from the HiFIS data, and the LiDAR data, were aligned to the same grid as the environmental and spectral predictor variables and averaged to 30 m resolution. CWC data were masked prior to averaging using the LiDAR-derived height mask described above in order to only analyze CWC data from fully-illuminated vegetation pixels for canopies taller than 2 m in height, thereby eliminating the contribution of grass cover, short shrubs, and non-forest canopy vegetation.

A data set comprised of each of the features described above was used to train the model on the CWC data that was collected by the CAO. This model was then applied to the entire feature space, which covers the full extent of California forests, in order to predict CWC in locations where the CAO did not collect data. Due to the large quantity of training data available, no imputation was performed on the input data set; any sample with a missing data value was simply excluded. In order to assess the accuracy of each model, an independent model with a random 90% of the training data was constructed and evaluated by comparison to the remaining 10% of the training data. For final map production, the model utilized all training data.

CWC Model

A deep learning model, also known as a multi-layer neural network, was used to model CWC across the state. The functional unit of a deep learning model is the neuron, in which a nonlinear activation function is applied to a linear combination of weights. By stacking multiple layers of neurons together, complex nonlinear systems can be accurately modeled. This work uses a feed-forward 4-layer network with a tanh activation function, implemented using the machine learning platform H2O with a Python interface (21). Through experimentation with holdout sets, two 200 neuron hidden layers and 50 epochs were selected for peak performance and computational efficiency.

Ten percent of the original aircraft CWC data were left out of the scaling step in order to validate the 2015 statewide CWC map. These validation data were selected randomly from aircraft coverage acquired throughout the State, and were comprised of 1.2 million aircraft-based measurements. Regression analyses showed an R^2 of 0.82 and root mean squared error (RMSE) of 0.45 L m^{-2} of forest canopy area (**Fig. S5**). Mean absolute deviation was 0.33 L m^{-2} . The deviation between the MAD and

RMSE is indicative of a relatively small number of outlier data points heavily contributing to model error. These results indicate that the statewide map reproduces the spatial and ecological patterns of canopy water content measured using the aircraft data.

We assessed the importance of environmental factors mediating the large-scale pattern in 2015 forest canopy water content (**Fig. S6**), using the Gedeon method implemented in the H2O platform (21, 22). Map coordinates accounted for a large proportion of the geographic variation in CWC. Elevation also played an important 10% role in mediating forest CWC. Following those three background factors, a suite of satellite vegetation measurements derived from the Landsat 8 Operational Land Imager (OLI) were important indicators of forest CWC variability. These metrics include the fractional cover of green leaf photosynthetic vegetation (PV), bare ground exposure, and shortwave-infrared reflectance, the latter being sensitive to canopy water content (13, 23). This suite of satellite-based vegetation measurements are critically important to scaling up the direct CWC observations from airborne imaging spectroscopy, and to providing retrospective estimates of changes in CWC. Beyond these main factors determining CWC variation, relative elevation - a metric often used as a surrogate for belowground water availability - as well as time since last fire each accounted for about 6% of the variation in the 2015 CWC map. Other indicators such as distance to and density of roads, and distance to nearest water body, each explained about 3-5% of the mapped CWC variation. It is important to note that the feature influence on any particular pixel varies, and consequently these feature contributions are a collective average throughout the state.

Retrospective Analysis

The model trained on the 2015 airborne mapping flights was used to create a series of retrospective maps for 2011, 2013 and 2014, each representing the same August time period sampled in 2015. The retrospective maps were created by using the same input data types, however the Landsat-based variables, as well as the number of years since the last fire, were modified to correspond to the data from each year. Landsat data from all years was processed using CLASlite with the same parameters as described above. Once static maps of each year were created, these were used to produce change maps by taking the percent difference between years on a pixel-by-pixel basis. **Fig. 3** (main text) shows the percent difference in CWC across the state for the years of 2011-2013, 2013-2014, and 2014-2015. Any pixel containing missing data from Landsat images for a single year (usually due to cloud-cover) was omitted from these maps. Areas reported as burned during each time interval by the U.S. Forest Service (Calfire: http://cdfdata.fire.ca.gov/incidents/incidents_current) were also excluded.

A histogram breakdown of the percent difference data for each time period is shown in **Fig. 5a** (main text). Calculated changes in water content within each time interval (pixels with at least 5% loss from **Fig. 3**, main text) are shown in terms of hectares or maximum number of trees affected in **Figs. 4a** and **b** (main text), respectively. Finally, the combined effect of water loss from each year, the progressive water stress, is shown in **Fig. 6** (main text), calculated as the sum of percent loss from each time period. Any pixel designated as burned between 2011 and 2015 was excluded from the **Fig. 6** (main text).

Forest Mask

We used the USGS LANDFIRE vegetation types (<http://landfire.cr.usgs.gov/viewer/>) coupled with LiDAR DTM and DSM data to create a mask of forest area in the State of California. Vegetation types listed by LANDFIRE as Agriculture, Barren, Developed, Herbaceous, Grassland, Non-vegetated, Open water, Quarries-Strip Mines-Gravel Pits, and Snow-Ice were excluded. Additionally, any pixels with difference between the DTM and DSM of less than 2 m were excluded. In total, 13.4 million hectares of California were considered as forested.

Tree Density Mapping

We mapped the density of trees across all forested regions of California using US Forest Service (USFS) Forest Inventory and Analysis (FIA) data. The number of trees per hectare recorded in the FIA plots ranged from 3-500 trees per hectare with a median value of 80 trees ha⁻¹ (**Fig. S13**). Using the approximate locations of all FIA plots in the state measured in or after the year 2000, we computed average tree density for 5,565 plots distributed throughout California. FIA plots are made up of four individual subplots of either 24.0 or 58.9 ft, arranged in a triangular pattern (24). Because the plot radius can vary, each tree in the database has an associated expansion factor giving the number of trees per acre that the tree represents. We summed expansion factors for all trees with a diameter at breast height (DBH) greater than 5" (12.7 cm) in each subplot, and then averaged the four subplot totals for each FIA plot. Using the approximate locations for each plot shared by FIA (**Fig. S14a**), we interpolated these point values using a circular moving average window of 7500 m diameter centered at each point on a grid of 2000 x 2000 m. The resulting map was then smoothed using a square mean kernel 16 km x 16 km across. Values were converted from trees per acre to trees per hectare, and all non-forested area was masked out to produce a final tree density map matched to the other statewide variables in our data (**Fig. S14b**).

The tree density map was then applied on a per-pixel basis to the data in **Figs. 3** and **6** (main text) to convert the number of acres at each loss interval to the maximum number of trees affected in each loss interval. Because the change in CWC from **Figs. 3** and **6** is an average over the pixel, the change in CWC could either be concentrated in a small number of trees, or evenly distributed throughout the pixel. Consequently the estimates of affected trees indicate the *maximum* number of impacted trees. These affected tree estimates are shown in **Fig. 5b** (main text), as well as the inset graph in **Fig. 6** (main text).

Evaluation of Progressive Water Stress (PWS) Map

We compared the modeled 30-m progressive water stress (PWS; Fig. 6; main text) from 2011 to 2015, to fine-resolution (2-m) CWC measurements in 2015 from airborne laser-guided imaging spectroscopy. Specifically, we overlaid the three large landscapes shown in Fig. 1 (main text) onto the PWS 2011-2015 map, and we calculated the spatial coefficient of variation (CV) in 2-m CWC within the 30-m PWS pixels. These three landscapes are typical of forests harboring relatively low, medium and high canopy water content in 2015. In medium to high forest CWC environments (Fig. 1; main text),

increasing 30-m resolution PWS (0% to > 30%) from 2011 to 2015 was closely associated with increasing spatial variation in CWC at 2-m resolution in 2015 (**Table S3**). This result is highly indicative of water content losses at the tree level, or at even finer sub-canopy scales. In contrast, the driest landscape in 2015 (Fig. 1; main text) was associated with nearly constant spatial variation in 2-m CWC, suggesting that water losses had occurred early in our time series (2011-2013). These findings show that progressive water stress is highly indicative of extensive crown-level canopy water loss, which in the field, would be an indicator of reduced canopy leaf area and tree mortality.

References

1. Asner GP, *et al.* (2012) Carnegie Airborne Observatory-2: Increasing science data dimensionality via high-fidelity multi-sensor fusion. *Remote Sensing of Environment* 124(0):454-465.
2. Asner GP (2009) Tropical forest carbon assessment: integrating satellite and airborne mapping approaches. *Environmental Research Letters* 3:1748-9326.
3. Asner GP, *et al.* (2011) High-resolution carbon mapping on the million-hectare Island of Hawaii. *Frontiers in Ecology and the Environment* 9(8):434-439.
4. Asner GP, *et al.* (2012) High-resolution mapping of forest carbon stocks in the Colombian Amazon. *Biogeosciences* 9(7):2683-2696.
5. Baccini A & Asner GP (2013) Improving pantropical forest carbon maps with airborne LiDAR sampling. *Carbon Management* 4(6):591-600.
6. Mascaro J, *et al.* (2014) A tale of two "forests": Random Forest machine learning aids tropical forest carbon mapping. *PLoS ONE* 9(1):e85993.
7. Asner GP, *et al.* (2014) Targeted carbon conservation at national scales with high-resolution monitoring. *Proceedings of the National Academy of Sciences* 111(47):E5016-E5022.
8. Colgan MS, Baldeck CA, Féret J-B, & Asner GP (2012) Mapping savanna tree species at ecosystem scales using support vector machine classification and BRDF correction on airborne hyperspectral and LiDAR data. *Remote Sensing* 4(11):3462-3480.
9. Green RO (2003) Understanding the three phases of water with imaging spectroscopy in the solar reflected energy spectrum. Ph.D. (University of California, Santa Barbara).
10. Asner GP (1998) Biophysical and Biochemical Sources of Variability in Canopy Reflectance. *Remote Sensing of Environment* 64(3):234-253.
11. Asner GP (2004) Biophysical remote sensing signatures of arid and semi-arid regions. *Remote Sensing for Natural Resources, Management and Environmental Monitoring: Manual of Remote Sensing*, ed Ustin SL (Wiley & Sons, New York), Vol 4, pp 53-109.
12. Kokaly RF, Asner GP, Ollinger SV, Martin ME, & Wessman CA (2009) Characterizing canopy biochemistry from imaging spectroscopy and its application to ecosystem studies. *Remote Sensing of Environment* 113(0):S78-S91.
13. Ceccato P, Flasse S, Tarantola S, Jacquemoud S, & Gregoire JM (2001) Detecting vegetation leaf water content using reflectance in the optical domain. *Remote Sensing of Environment* 77(1):22-33.
14. Asner GP & Martin RE (2008) Spectral and chemical analysis of tropical forests: Scaling from leaf to canopy levels. *Remote Sensing of Environment* 112(10):3958-3970.
15. Asner GP, *et al.* (2007) Carnegie Airborne Observatory: in-flight fusion of hyperspectral imaging and waveform light detection and ranging for three-dimensional studies of ecosystems. *Journal of Applied Remote Sensing* 1:013536.
16. Dahlin K, Asner GP, & Field CB (2011) Environmental filtering and land-use history drive patterns in biomass accumulation in a mediterranean-type landscape. *Ecological Applications*.
17. Asner GP, Knapp DE, Balaji A, & Paez-Acosta G (2009) Automated mapping of tropical deforestation and forest degradation: CLASlite. *Journal of Applied Remote Sensing* 3:033543.
18. Roberts DA, Green RO, & Adams JB (1997) Temporal and spatial patterns in vegetation and atmospheric properties from AVIRIS. *Remote Sensing of Environment* 62(3):223-240.
19. Roberts DA, Green, R.O., Sabol, D.E., and Adams, J.B. (1993) Temporal changes in endmember abundances, liquid water and water vapor over vegetation at Jasper Ridge. Fourth Annual JPL Airborne Geoscience Workshop, ed Green RO, pp 153-156.

20. Roberts D (1991) Separating Spectral Mixtures of Vegetation and Soils. Ph. D. Dissertation (University of Washington, Seattle, WA).
21. H2O-team (2015) H2O: Scalable Machine Learning. version 3.1.0.99999.
22. Gedeon TD (1997) Data mining of inputs: analysing magnitude and functional measures. *International Journal of Neural Systems* 8(02):209-218.
23. Ustin S, et al. (1996) Estimating Canopy Water Content of Chaparral Shrubs Using Optical Methods. *Summaries of the Sixth Annual JPL Airborne Earth Science Workshop*, ed Green RO (NASA JPL), pp 235-238.
24. Woodall CW, et al. (2010) *The Forest Inventory and Analysis Database Version 4.0: Database Description and Users Manual for Phase 3* (U.S. Department of Agriculture, Newtown Square, PA), (Service USF).

Table S1. Geospatial datasets used for statewide mapping of California.

Parameter	Description	Reference
Map Coordinates	UTM (Zone 10 North) Coordinates at 30-meter intervals	Calculated to cover the study area
Elevation (m a.s.l.)	Elevation, meters above sea level	NED: 1/3-Arc Second National Elevation Dataset (NED), U.S. Department of Interior, Geological Survey. Available: http://nationalmap.gov/
Slope and Aspect (degrees)	Slope and Aspect of terrain	Calculated from elevation
Relative Elevation; and Distance to Water Body (m)	Elevation relative and distance to the water level in the nearest stream	Calculated from Stream/River data from U.S. Census Bureau Topologically Integrated Geographic Encoding and Referencing (TIGER) 2014; Available at: ftp://ftp2.census.gov/geo/tiger/
Reflectance 1.57-1.65 and 2.11-2.29 μm	Landsat-8 Reflectance for 1.57-1.65 μm region at 30 meters*	Landsat-8 radiance data acquired through Google Earth Engine, calibrated to reflectance using CLASlite
Vegetation Fractional Cover (%)	Photosynthetic Vegetation, Non-photosynthetic Vegetation, Bare Substrate	Calculated using CLASlite software; Asner et al. 2009.
Road Distance (km) and Density (0-1)	Distance from nearest road and density of roads calculated as fraction of road in a 1200 m^2 moving window averaging 30x30m pixels.	Calculated from road data from U.S. Census Bureau Topologically Integrated Geographic Encoding and Referencing (TIGER) 2014; Available at: ftp://ftp2.census.gov/geo/tiger/
Potential Solar Insolation (kW h m^2)	Potential Solar Insolation (direct and diffuse) for March 21, June 21, September 21, and December 21	Modeled based on elevation and using the SAGA GIS Potential Insolation module (SAGA-Python v0.37)
Time since Fire (yr)	Number of years since a fire occurrence	CALFIRE: http://cdfdata.fire.ca.gov/incidents/

* for the year 2011, Landsat-5 radiance data were used with reflectance values of 1.55-1.75 and 2.08-2.35 mm. These minor deviations in the longer wavelengths do not influence the near infrared (NIR) regions where canopy water is active in the spectrum.

Table S2. Woody vegetation types derived from the USFS LANDFIRE database (<http://landfire.cr.usgs.gov/viewer/>) and arranged by decreasing progressive water stress (PWS, %). Note that only woody canopies with a height of at least 2 m are included in the study. PWS data are means and variance within each class. The total area affected is listed in thousands of hectares, and the elevation (m) of the vegetation type (mean and 5th and 95th percentiles) is shown.

Forest Type	PWS (%)	Area	Elevation (m)
Pacific Coastal Scrub	19.1±13.5	149.6	313 (59-672)
Lower Montane Blue Oak Forest	19.0±13.1	100.3	446 (117-1001)
Southern Dry Mesic Chaparral	17.2±13.3	162.4	646 (145-1204)
California Mesic Chaparral	17.0±14.3	426.9	515 (58-1301)
Conifer Oak Forest/Woodland	16.6±12.5	908.4	541 (158-1045)
Xeric Serpentine Chaparral	16.6±12.8	11.5	703 (91-1343)
Northern/Central Dry Mesic Chaparral	16.3±13.1	436.6	513 (75-1054)
Western Oak Woodland/Savanna	16.2±13.1	153.6	553 (127-1429)
Mediterranean Mesic Serpentine Chaparral	15.5±13.1	65.7	768 (229-1770)
Low Sagebrush Shrubland	14.5±14.2	56.6	2250 (1631-3503)
Semi-Desert Chaparral	13.7±12.6	55.6	878 (56-1876)
California Coastal Live Oak Woodland	13.4±11.3	16.5	328 (57-743)
Inter-Mountain Basins Montane Riparian Woodland	13.3±13.1	16.3	1634 (1006-2439)
Mountain Mahogany Woodland	13.3±13.4	47.1	2411 (1512-3060)
Central Valley Riparian Forest	13.3±11.8	16.5	115 (13-193)
California Mixed Evergreen Forest	12.9±11.6	463.9	632 (131-1526)
California Montane Chaparral	12.6±13.1	484.5	1417 (225-2536)
Mediterranean Subalpine Woodland	12.4±11.9	80.7	2988 (2363-3303)
Subalpine Lodgepole Pine Forest	12.4±10.1	82.3	2787 (2199-3072)
Pinyon Juniper Forest	12.4±12.5	176.7	2070 (1454-2663)
Big Sagebrush Shrubland	12.2±11.0	162.9	1604 (1305-2172)
Mediterranean California Mixed Oak Woodland	11.9±10.8	494.5	1101 (499-1808)
Lower Montane Conifer Oak Forest	11.8±10.1	108.3	592 (193-1031)
Western Oak Woodland	11.7±11.8	22.5	785 (350-1143)
Aspen Forest	11.4±11.3	34.0	2447 (1971-2852)
Mid Elevation Desert Shrubland	11.3±13.1	117.4	1521 (814-2362)
Western Montane Riparian Woodland	11.2±11.8	65.1	1358 (233-2440)
North Pacific Oak Woodland	11.0±10.1	72.0	565 (130-1039)
Mediterranean California Red Fir Forest	10.9±9.9	780.9	2264 (1788-2762)
Northern California Mesic Subalpine Woodland	10.8±9.2	22.9	2205 (1726-2867)
Montane Riparian Systems	10.5±10.3	294.7	1035 (101-2480)
Conifer Oak Forest	10.1±9.5	37.0	708 (270-1038)
Lower Montane Conifer Forest	9.7±9.6	197.1	844 (322-1382)
Lower Montane Black Oak, Conifer Forest	9.6±8.4	10.5	654 (179-1224)
California Coastal Redwood Forest	9.0±9.1	710.7	294 (68-574)
Creosote Shrubland	8.9±11.7	215.5	710 (232-1152)
Montane Jeffrey Pine Woodland	8.0±9.7	607.4	1822 (1197-2468)
Dry Mesic Mixed Conifer Forest	7.9±8.7	1,234.3	1048 (556-1700)
Mixed Conifer, Western White Fir Forest	7.5±8.4	1,731.8	1586 (1109-2130)
Western White Pine, White Fir Forest	7.4±7.6	17.0	2014 (1659-2348)
Mixed Evergreen Forest	6.7±7.9	728.1	605 (186-1089)
Juniper Woodland	5.9±6.5	37.9	1537 (1317-1784)
Upper Montane Serpentine Mixed Conifer Woodland	5.3±5.7	43.2	1220 (645-1561)
Ponderosa Pine Forest, Woodland	5.1±7.1	212.5	1481 (1132-1839)
Lower Montane Serpentine Mixed Conifer Woodland	4.2±4.9	22.0	898 (412-1294)

Table S3. Coefficient of variation (CV) of 2-m resolution canopy water content (CWC) as observed using airborne laser-guided spectroscopy in 2015 at differing levels of progressive water stress (PWS) mapped at 30-m resolution from 2011 to 2015.

Progressive Water Stress (30-m map)	CV of 2-m Airborne Canopy Water Content (CWC) Data		
	Low	Medium	High
> 0%	35.7%	41.7%	24.3%
> 10%	35.8%	44.8%	27.4%
> 20%	36.6%	55.2%	31.1%
> 30%	37.4%	75.2%	32.8%

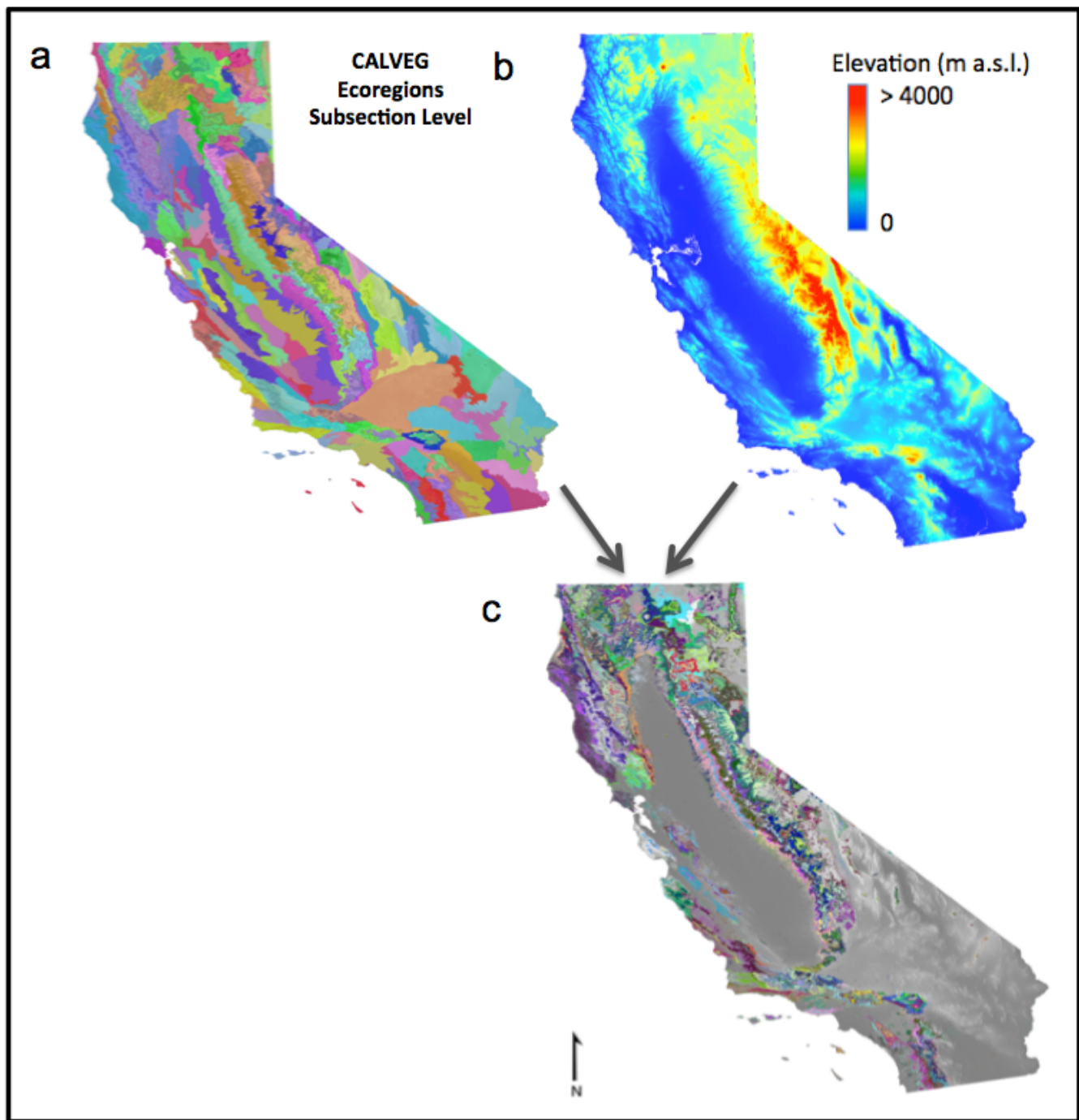


Fig. S1. **a)** Pre-stratification of the airborne sampling region using information of California ecosystems from CALVEG and **b)** Elevation from the USGS NED elevation data for the conterminous United States. These data sets were intersected creating one map (**c**) with 1,337 unique classes within the forested areas of California.

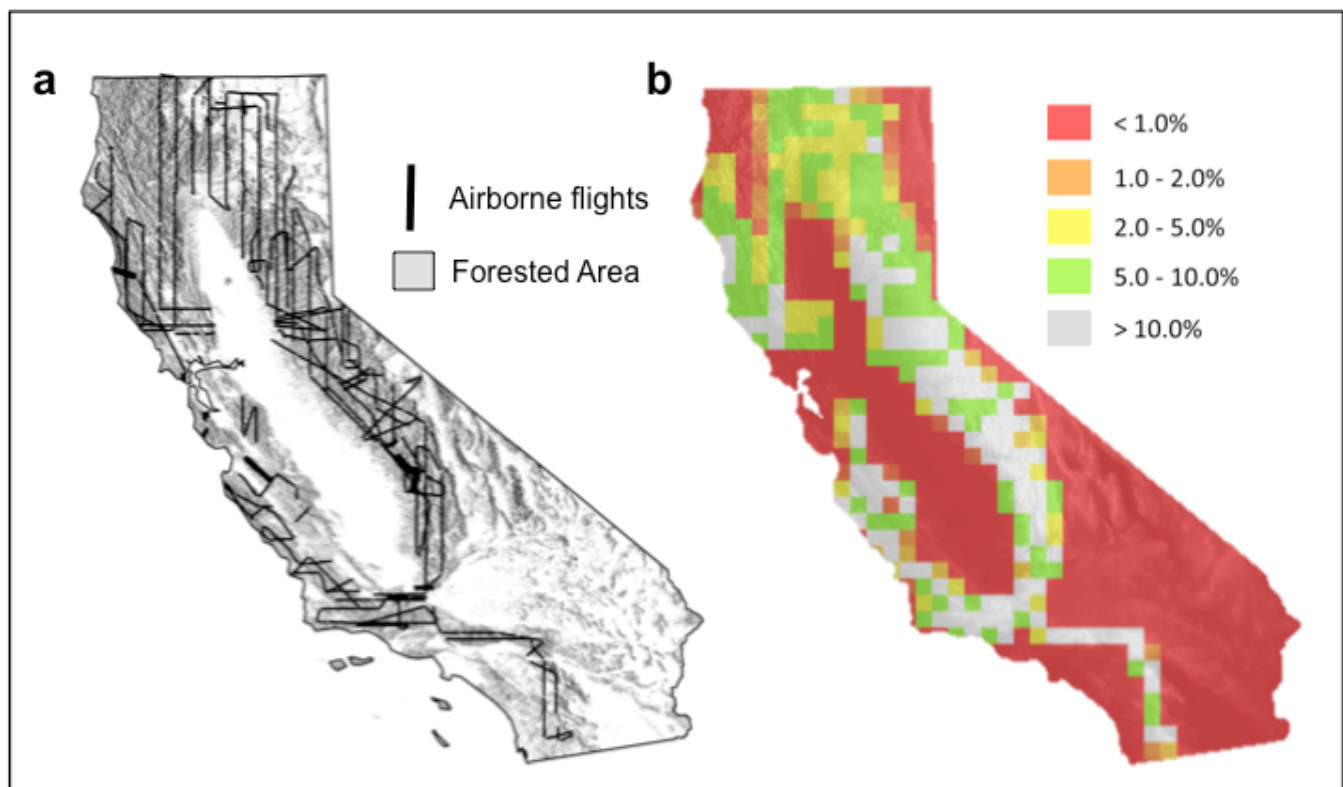


Fig. S2. **a)** Airborne Light Detection and Ranging (LiDAR) from the Carnegie Airborne Observatory was used to sample the region as shown in black lines. Total LiDAR observation coverage for this study was 1.8 million hectares. **b)** Percentage coverage of each 25 x 25 km sampling grid cell.

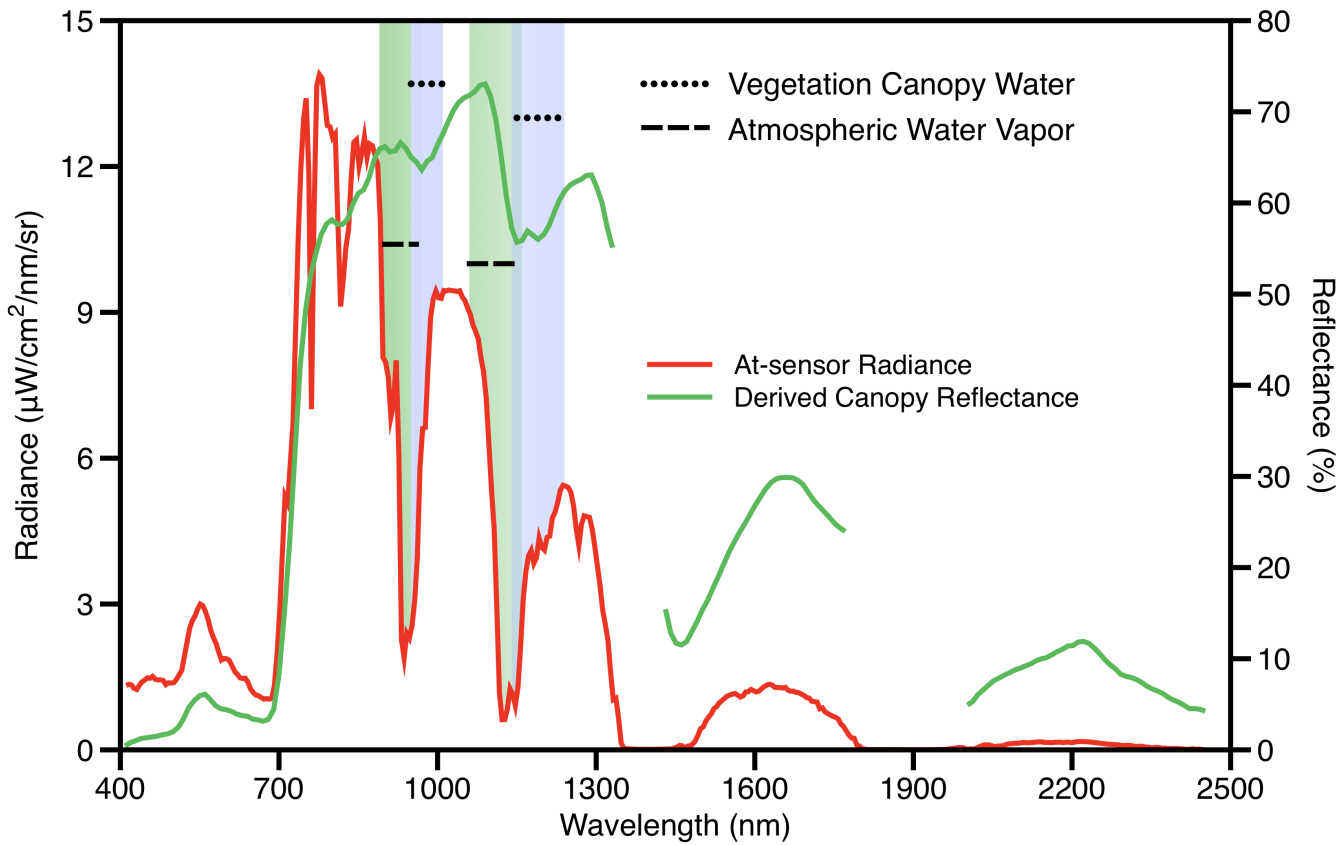


Fig. S3. Spectroscopic remote sensing of vegetation canopy water content (CWC) is made possible by the absorption of solar radiation based on the volume and mass concentration of water molecules in the canopy. The fundamental measurement is the spectral radiance (red line; units of $\mu\text{W cm}^{-2} \text{nm}^{-1} \text{sr}^{-1}$) showing the location of the strong liquid absorption features centered on 980 and 1160 nm. Atmospheric water vapor is also expressed in the radiance spectrum, centered at 940 and 1140 nm. Following correction for illumination and the atmospheric the apparent surface reflectance is retrieved with corresponding illumination and observation geometry (green line; units of % reflectance). The depth of the liquid water features in the reflectance are measured with spectral fitting and are related to total CWC.

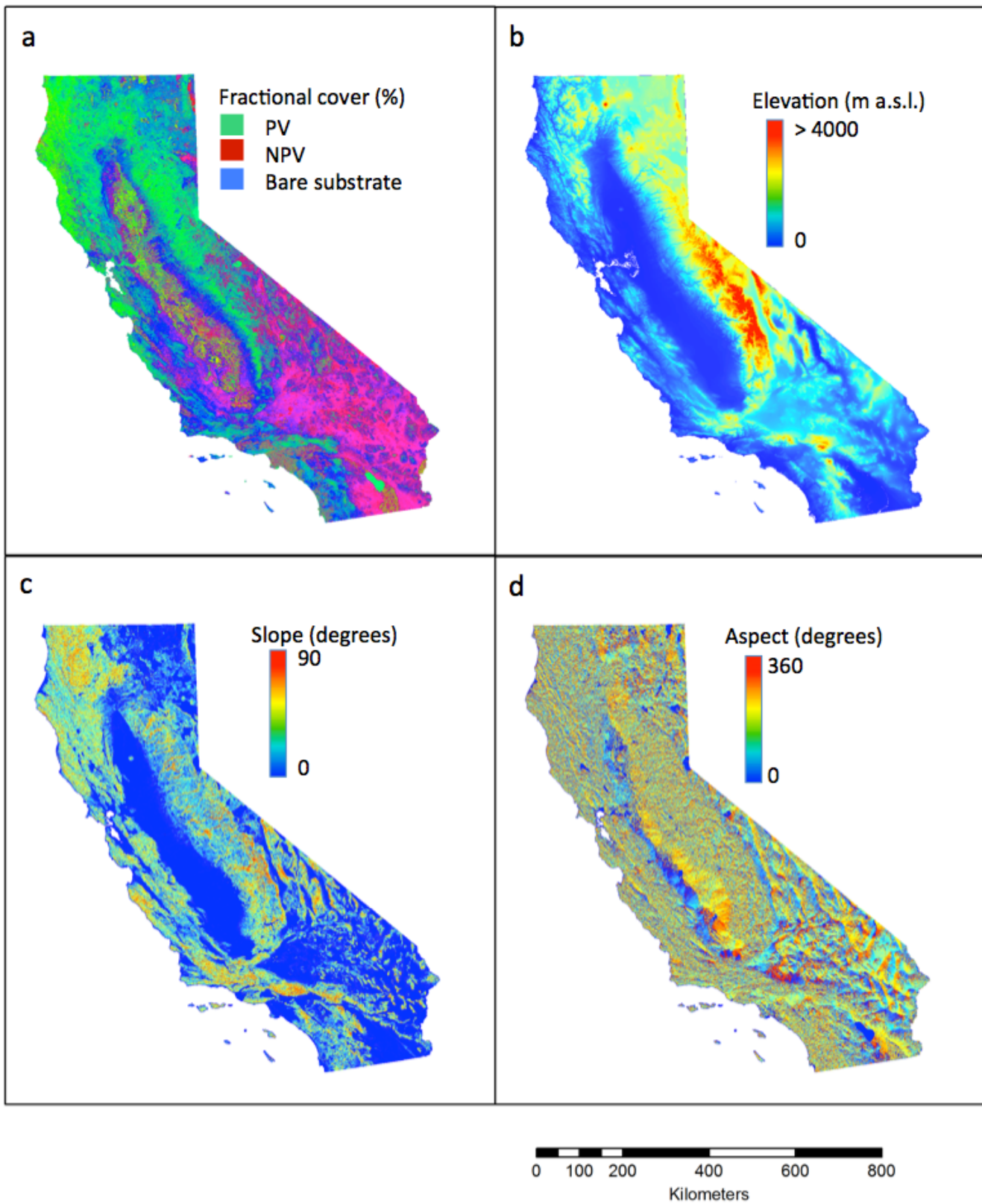


Fig. S4 a-d. Geospatial datasets used as inputs for statewide mapping. **a)** Fractional cover (%); green is photosynthetic vegetation (PV) , red is non-photosynthetic vegetation, blue is bare substrate; **b)** elevation (m a.s.l.); **c)** slope (degrees) and **d)** aspect (degrees).

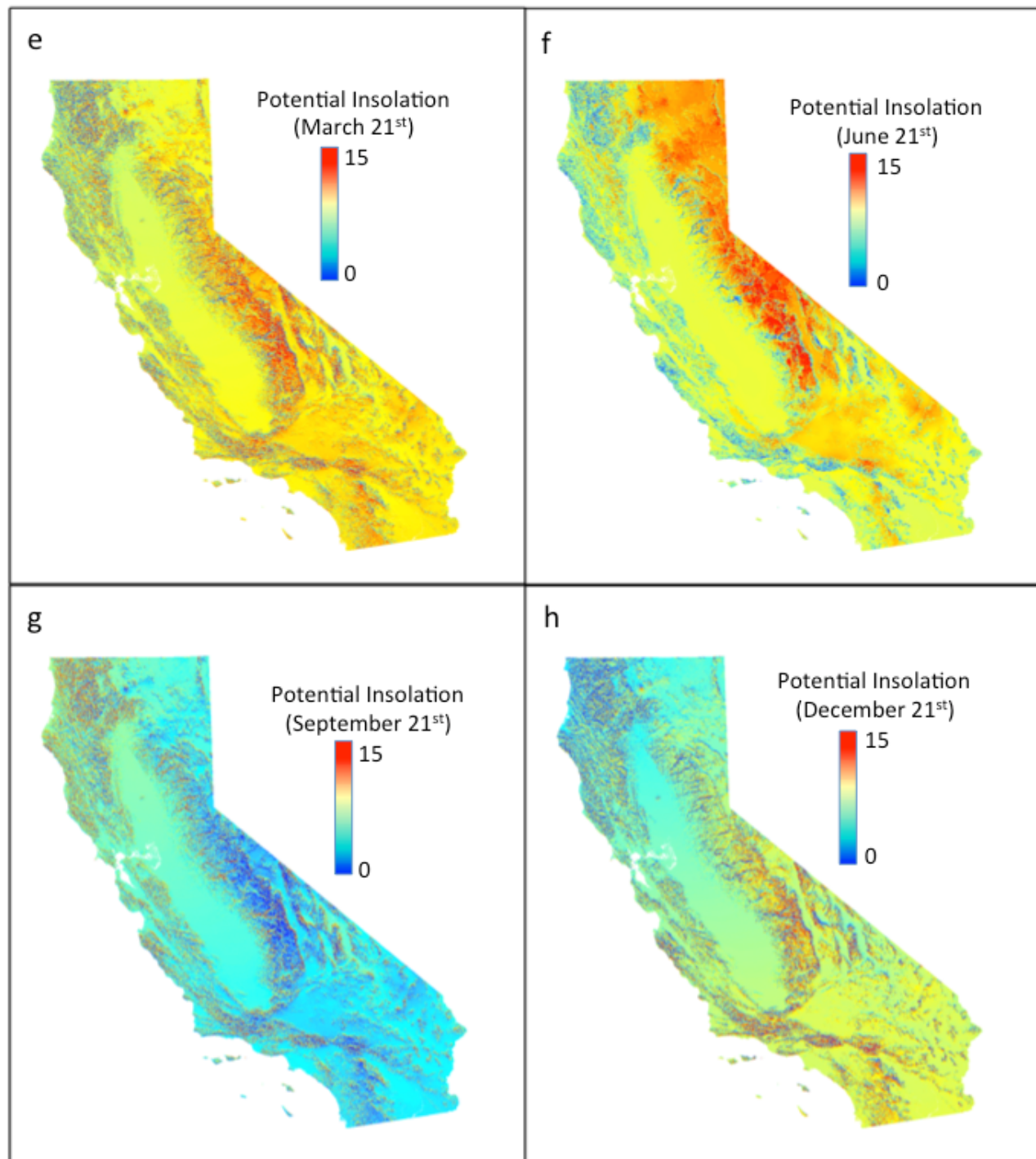


Fig. S4 e-h. Geospatial datasets used as inputs for statewide mapping continued. Potential insolation for **e)** March 21st; June 21st; **g)** September 21st; and **h)** December 21st.

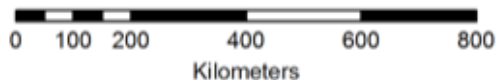
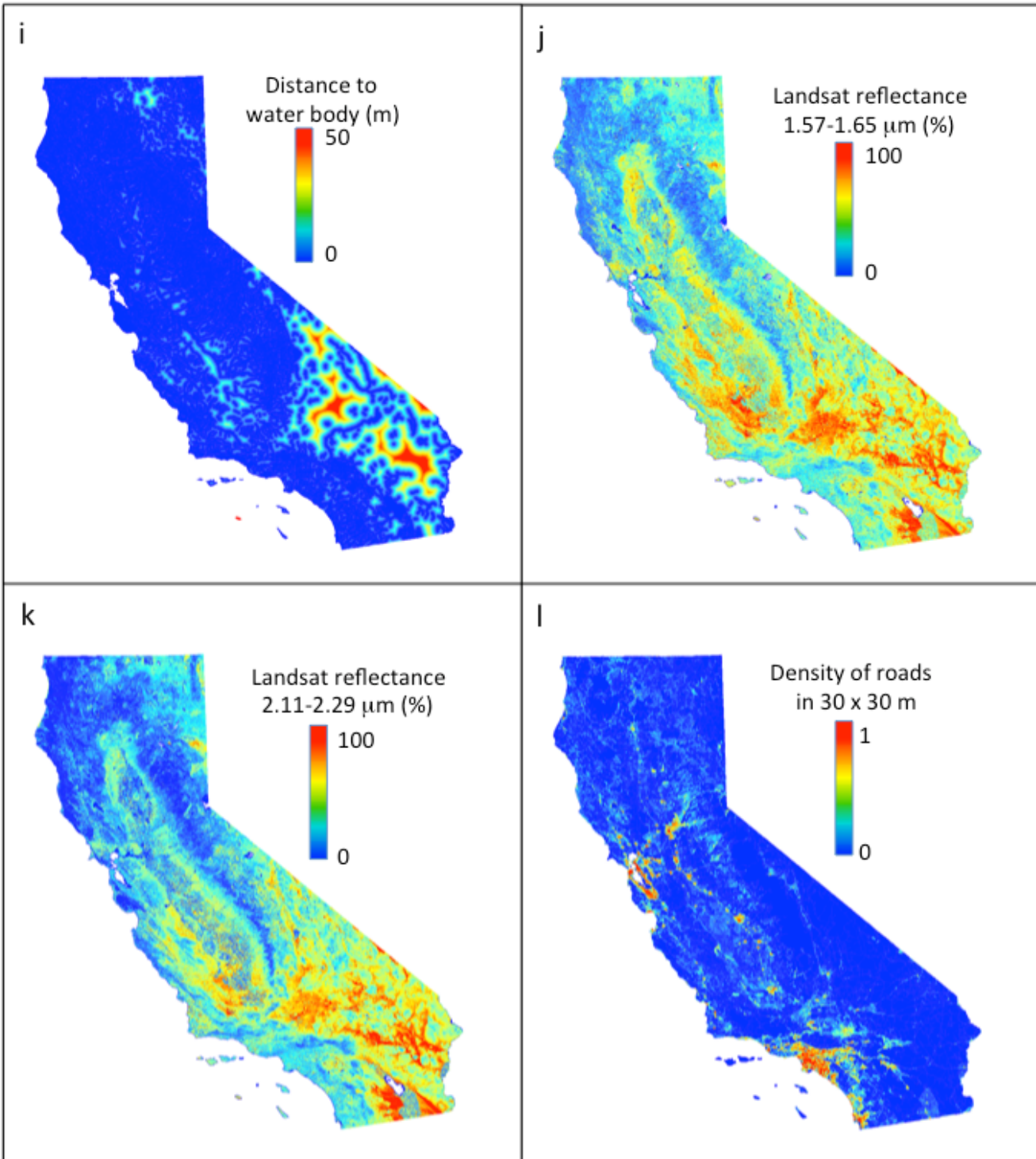


Fig. S4 i-l. Geospatial datasets used as inputs for statewide mapping continued. **i)** distance to a water body (i.e. stream, river, lake); **j)** Landsat-8 reflectance values (%) in the SWIR-1 region (1.57-1.65 μm), **k)** Landsat-8 reflectance values (%) in the SWIR-2 region (2.11-2.29 μm); **l)** Density of roads calculated as fraction of road in a 1200 m^2 moving window averaging 30x30m pixels.

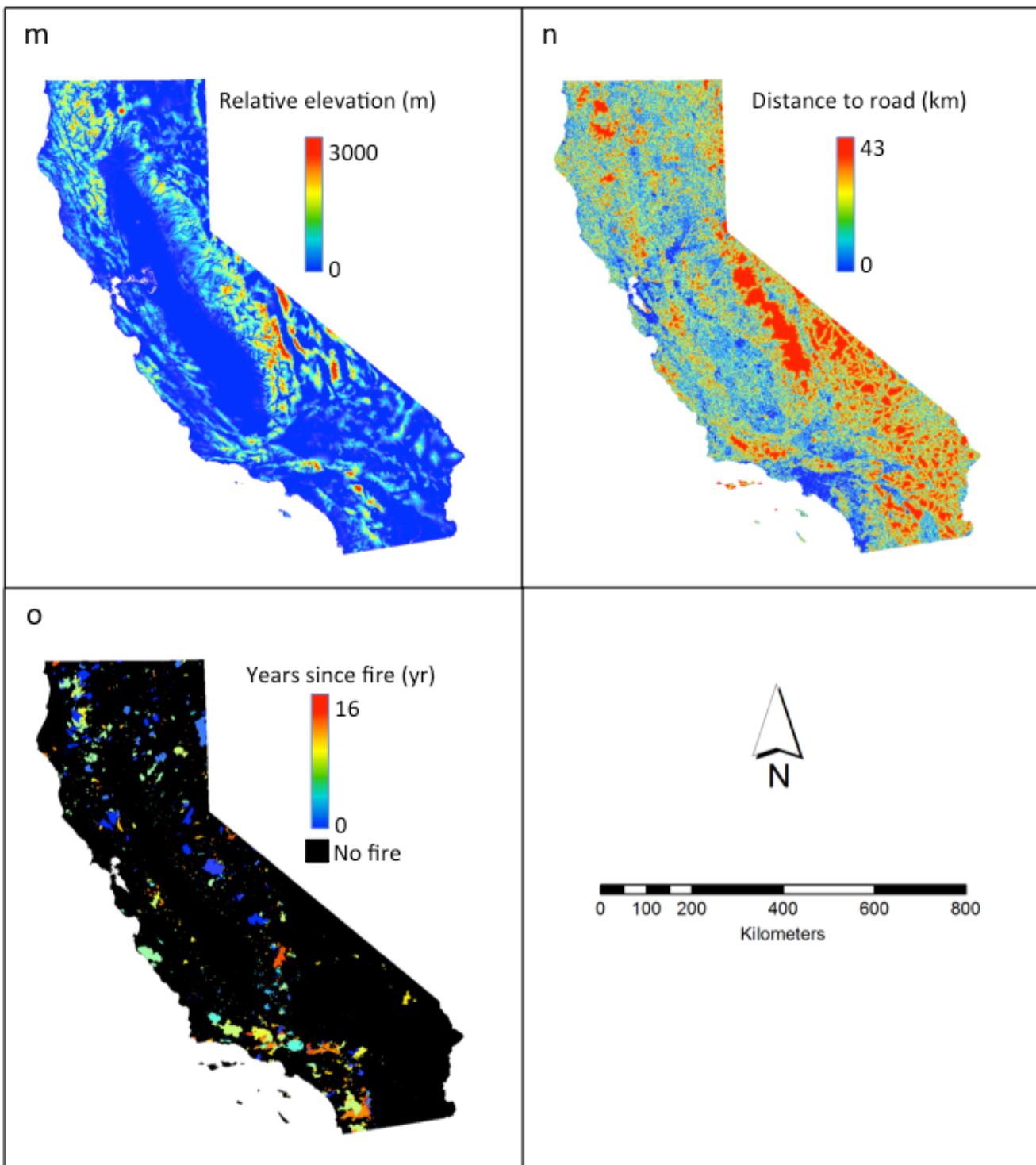


Fig. S4 m-o. Geospatial datasets used as inputs for statewide mapping continued. **m)** relative elevation (m) above the nearest stream, river or other water body; **n)** distance to road (km); and **o)** year since last fire as reported in the CALFIRE current fire monitoring system, black indicates there was no fire recorded since before the year 2000 when the database began tracking fires.

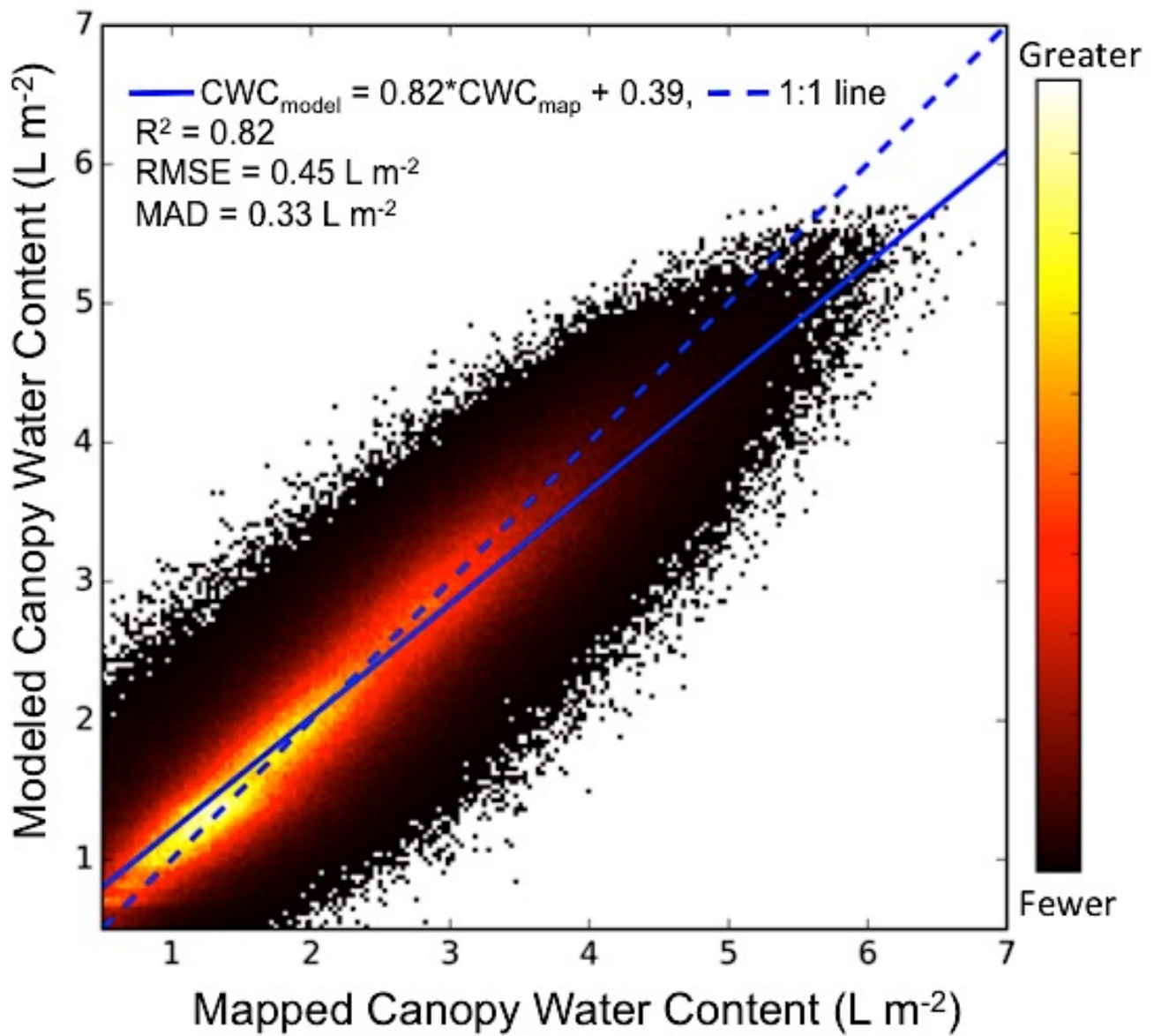


Fig. S5. Comparison of mapped versus modeled canopy water content (CWC; L m^{-2}). Color bar indicates the number of mapped pixels within a bin size of 0.03 L m^{-2} on a linear scale ranging from fewer (dark colors) to greater (light colors). Due to the large data volume, only bins with at least three pixels are shown. Total number of map pixels shown is 1.2 million. R^2 is the correlation coefficient, RMSE is root mean square error, and MAD is mean absolute deviation.

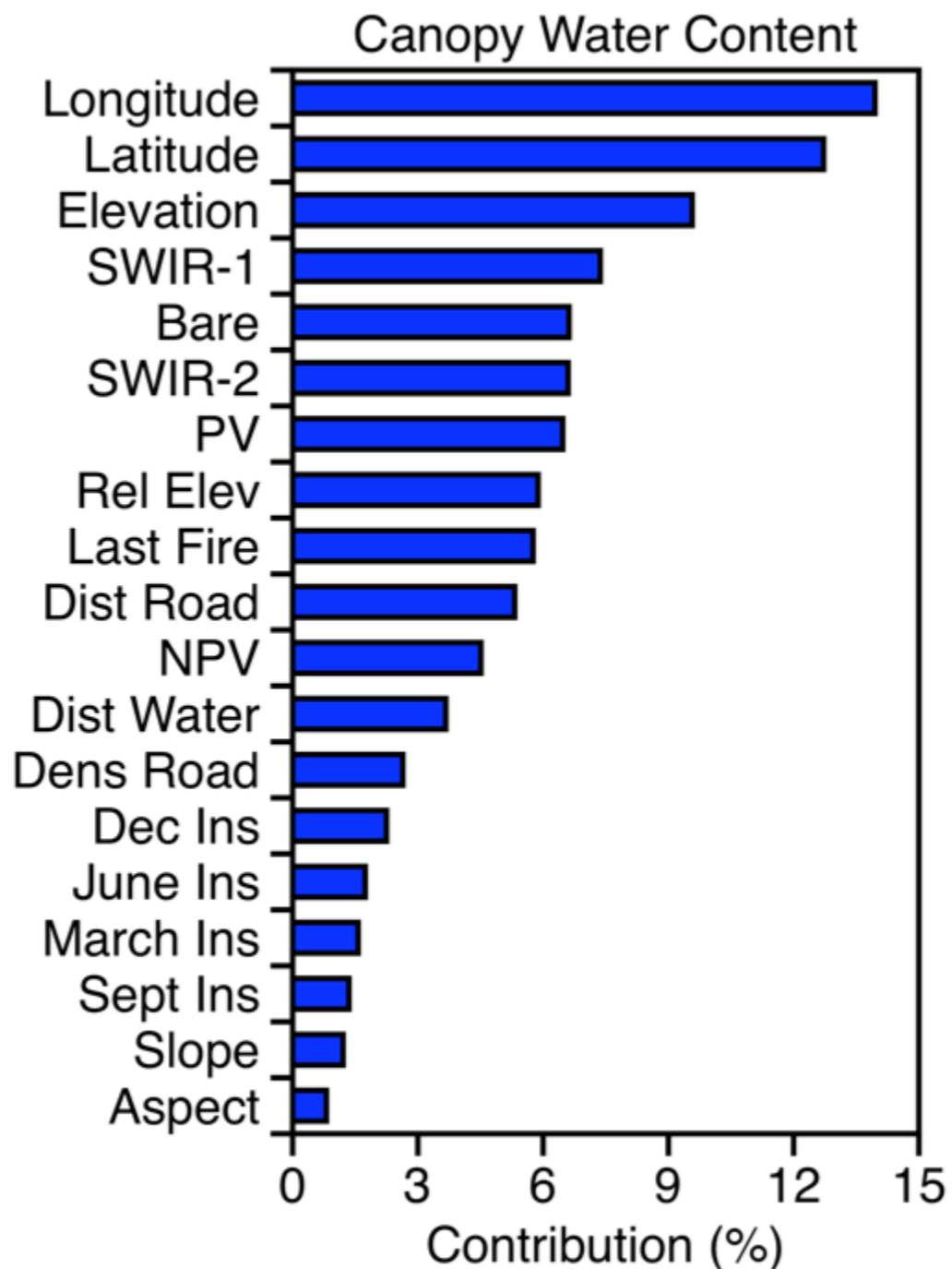


Fig. S6. Relative importance of environmental factors as determined by the deep learning model mediating the large-scale pattern in 2015 forest canopy water content.

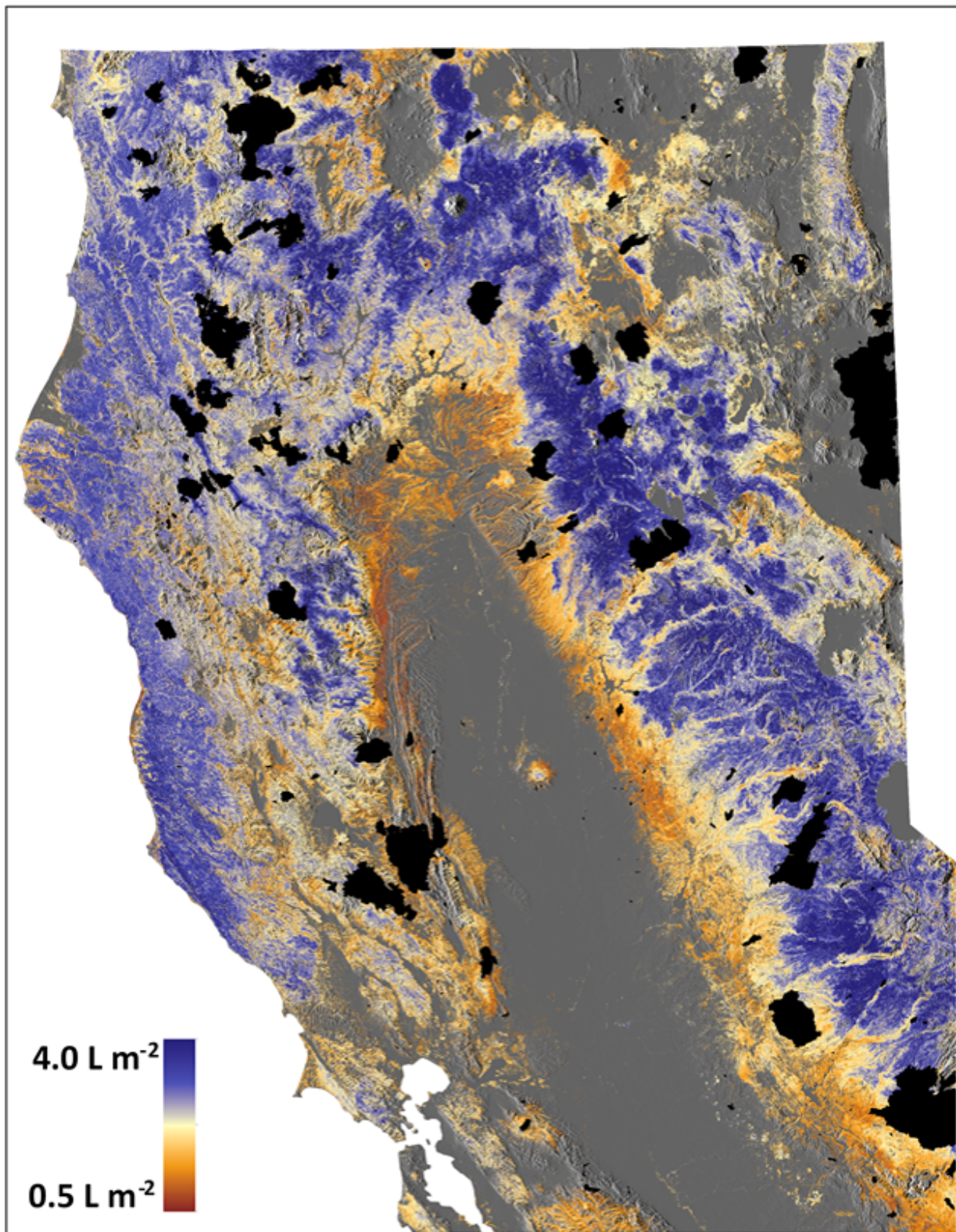


Fig. S7. Forest canopy water content reported in liters per square meter (L m^{-2}) for northern California as of August 2015. Black areas indicate fire extents reported between 2011 and 2015 by the U.S. Forest Service. See Fig. 2 of the main text for the entire map of California.

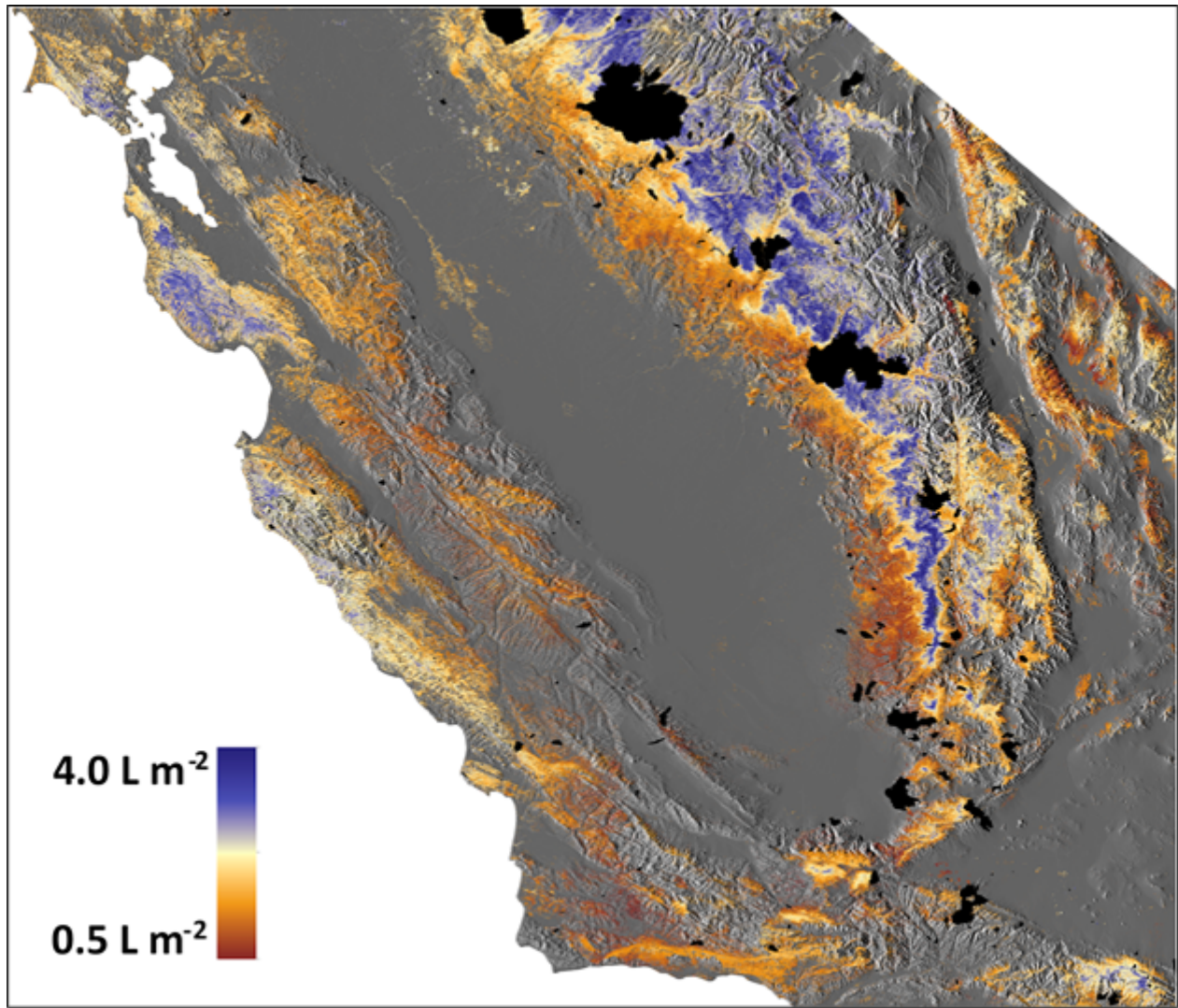


Fig. S8. Forest canopy water content reported in liters per square meter (L m^{-2}) for central California as of August 2015. Black areas indicate fire extents reported between 2011 and 2015 by the U.S. Forest Service. See Fig. 2 of the main text for the entire map of California.

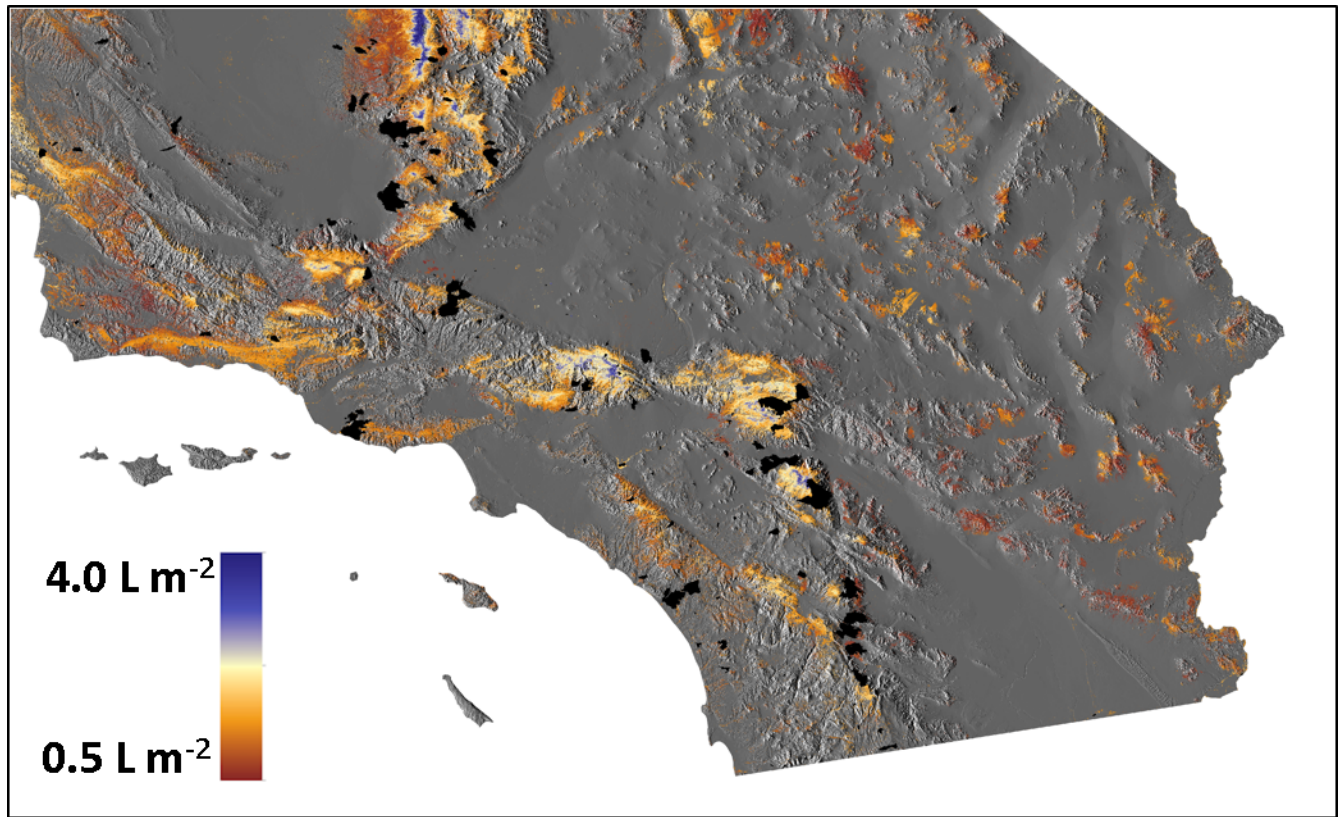


Fig. S9. Forest canopy water content reported in liters per square meter (L m^{-2}) for southern California as of August 2015. Black areas indicate fire extents reported between 2011 and 2015 by the U.S. Forest Service. See Fig. 2 of the main text for the entire map of California.

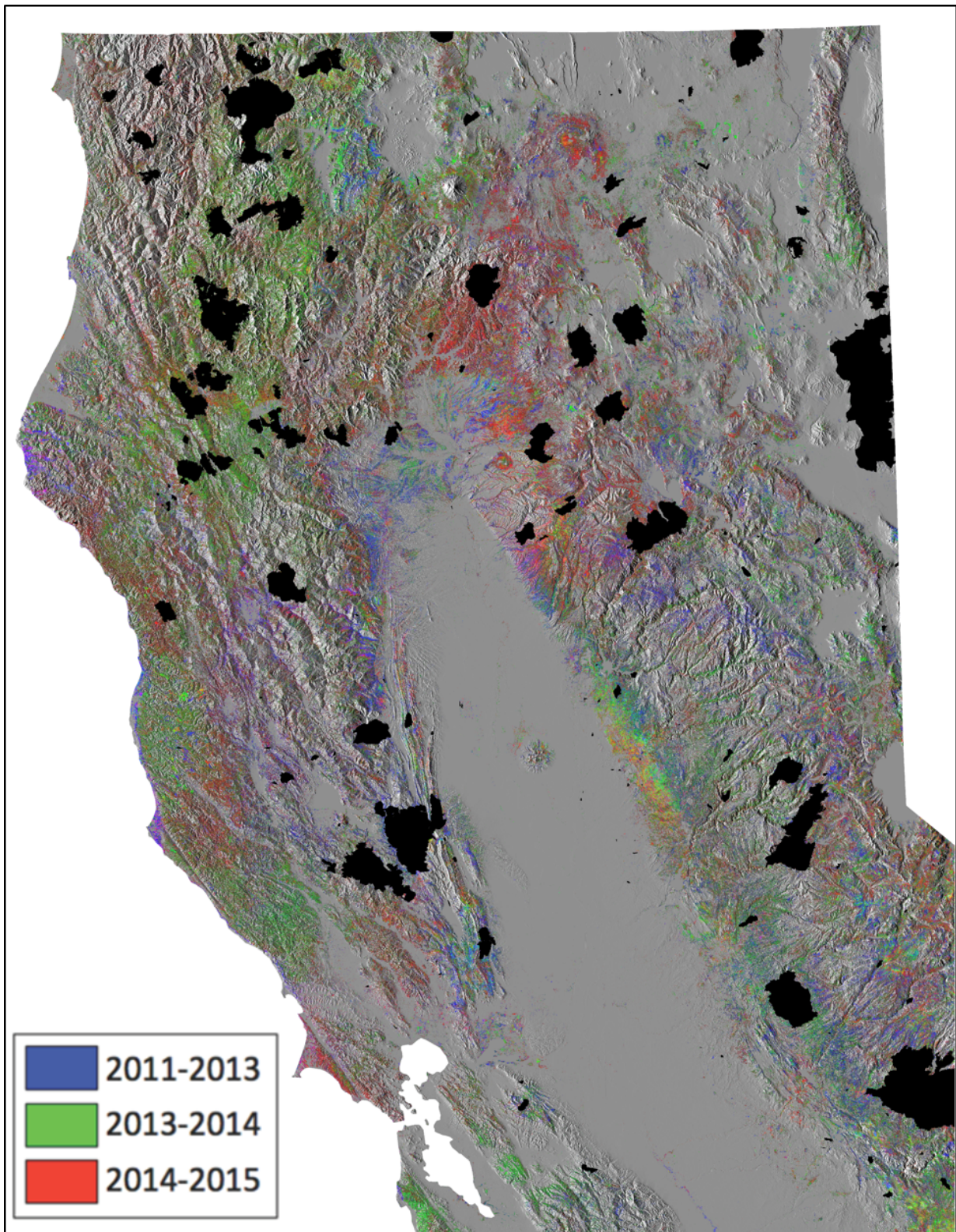


Fig. S10. The geography of forest canopy water stress for the period 2011 to 2015, partitioned spatially by onset period of observation, for northern California. Only water losses of at least 5% per observation interval are displayed. Black areas indicate fire extents reported between 2011 and 2015 by the U.S. Forest Service. See Fig. 4 of the main text for the entire map of California

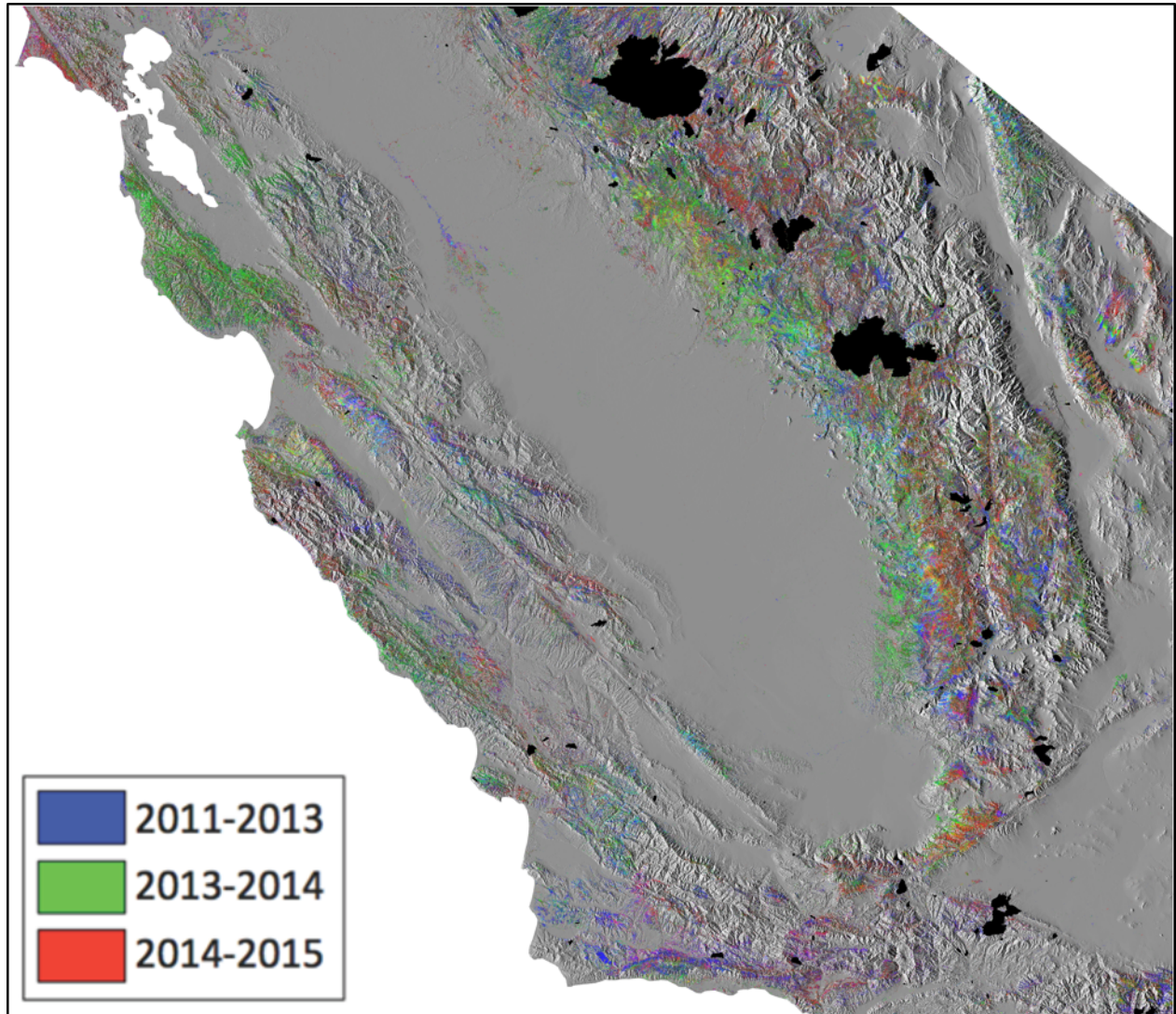


Fig. S11. The geography of forest canopy water stress for the period 2011 to 2015, partitioned spatially by onset period of observation, for central California. Only water losses of at least 5% per observation interval are displayed. Black areas indicate fire extents reported between 2011 and 2015 by the U.S. Forest Service. See Fig. 4 of the main text for the entire map of California.

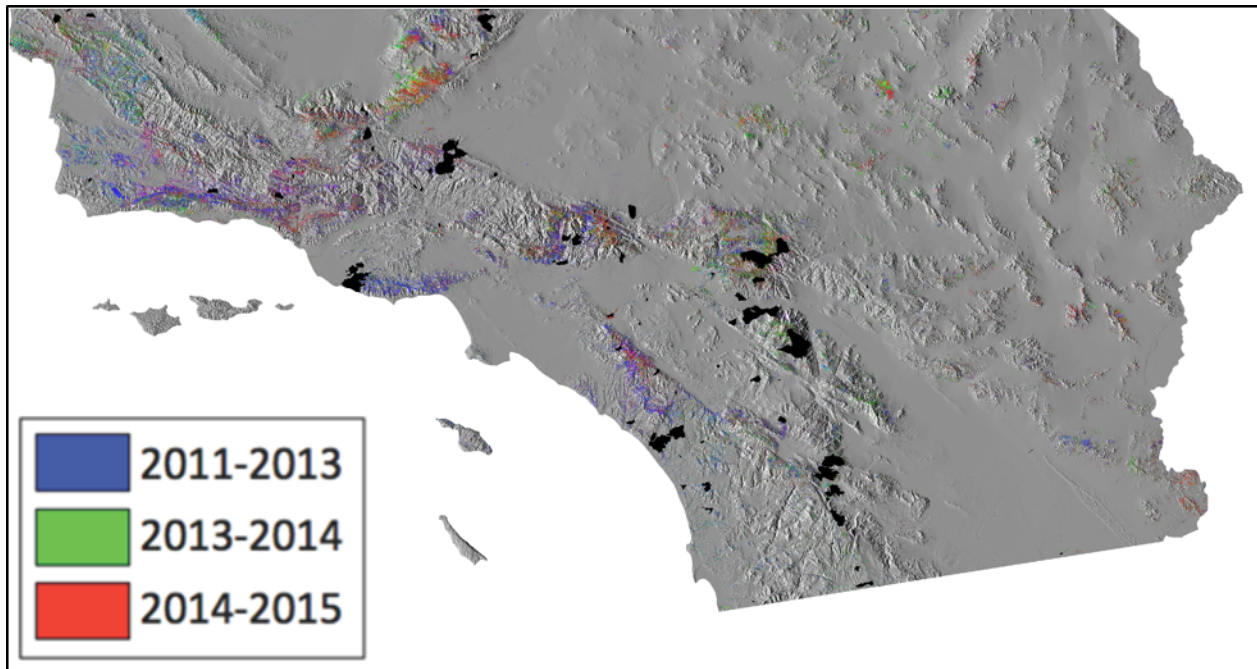


Fig. S12. The geography of forest canopy water stress for the period 2011 to 2015, partitioned spatially by onset period of observation, for southern California. Only water losses of at least 5% per observation interval are displayed. Black areas indicate fire extents reported between 2011 and 2015 by the U.S. Forest Service. See Fig. 4 of the main text for the entire map of California.

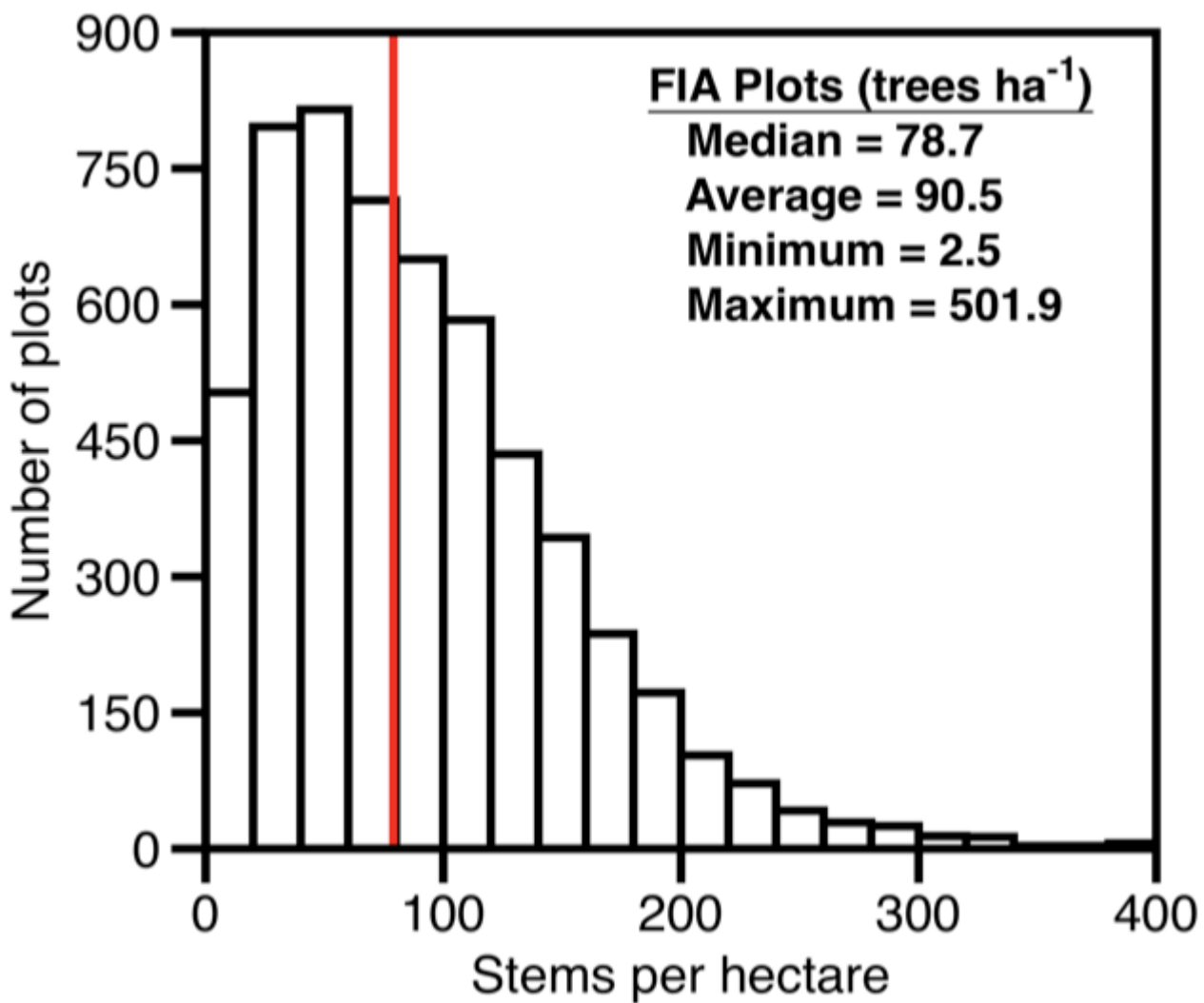


Fig. S13. Number of trees with diameter > 12.7 cm recorded in FIA vegetation survey plots.

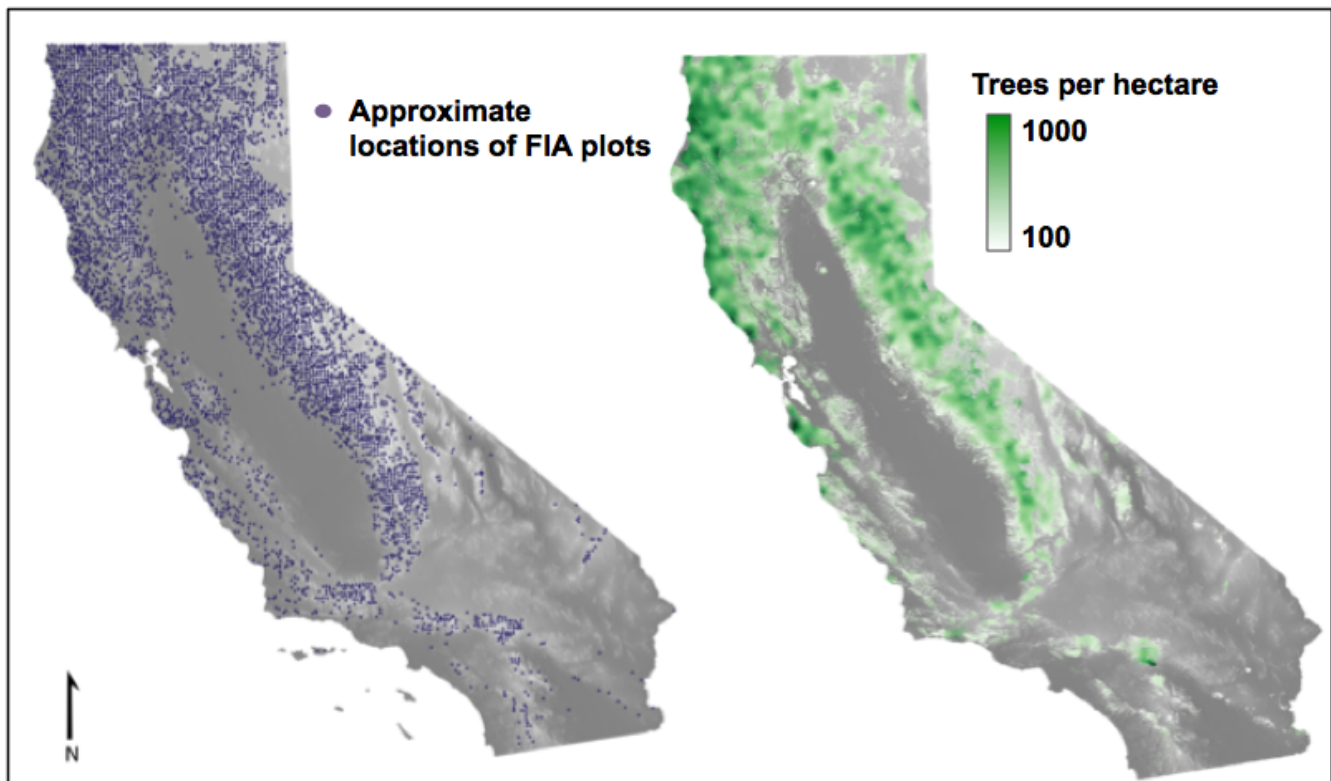


Fig. S14. Tree density [trees greater than 12.7 cm diameter] map and the location of plots used in the calculation. a) Approximate location of FIA vegetation survey plots and b) modeled tree density.

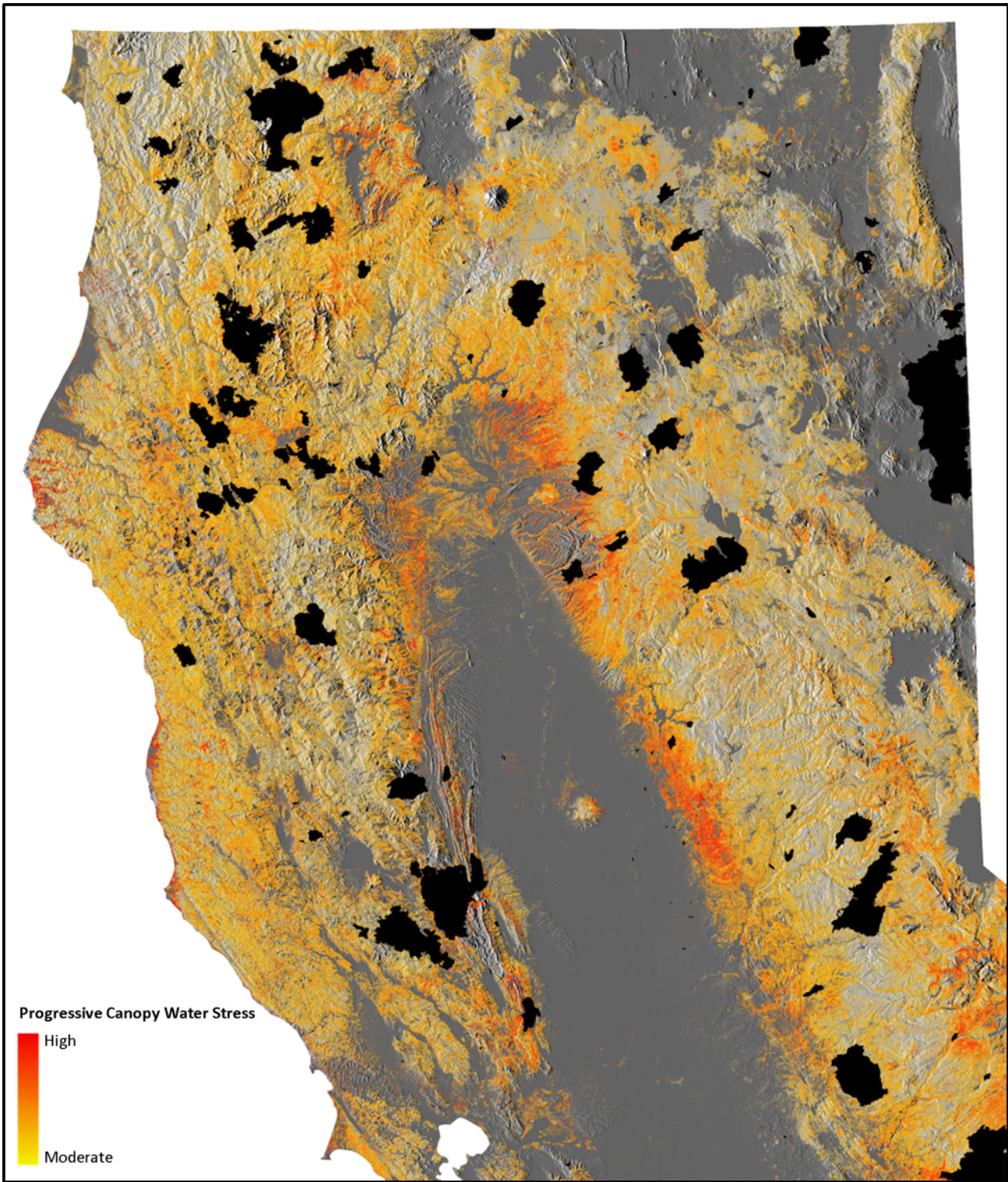


Fig. S15. Progressive forest canopy water stress for the years 2011 to 2015, computed as the sum of the percentage losses per observation period, for northern California. Black areas indicate fire extents reported between 2011 and 2015 by the U.S. Forest Service. See Fig. 6 of the main text for the entire map of California.

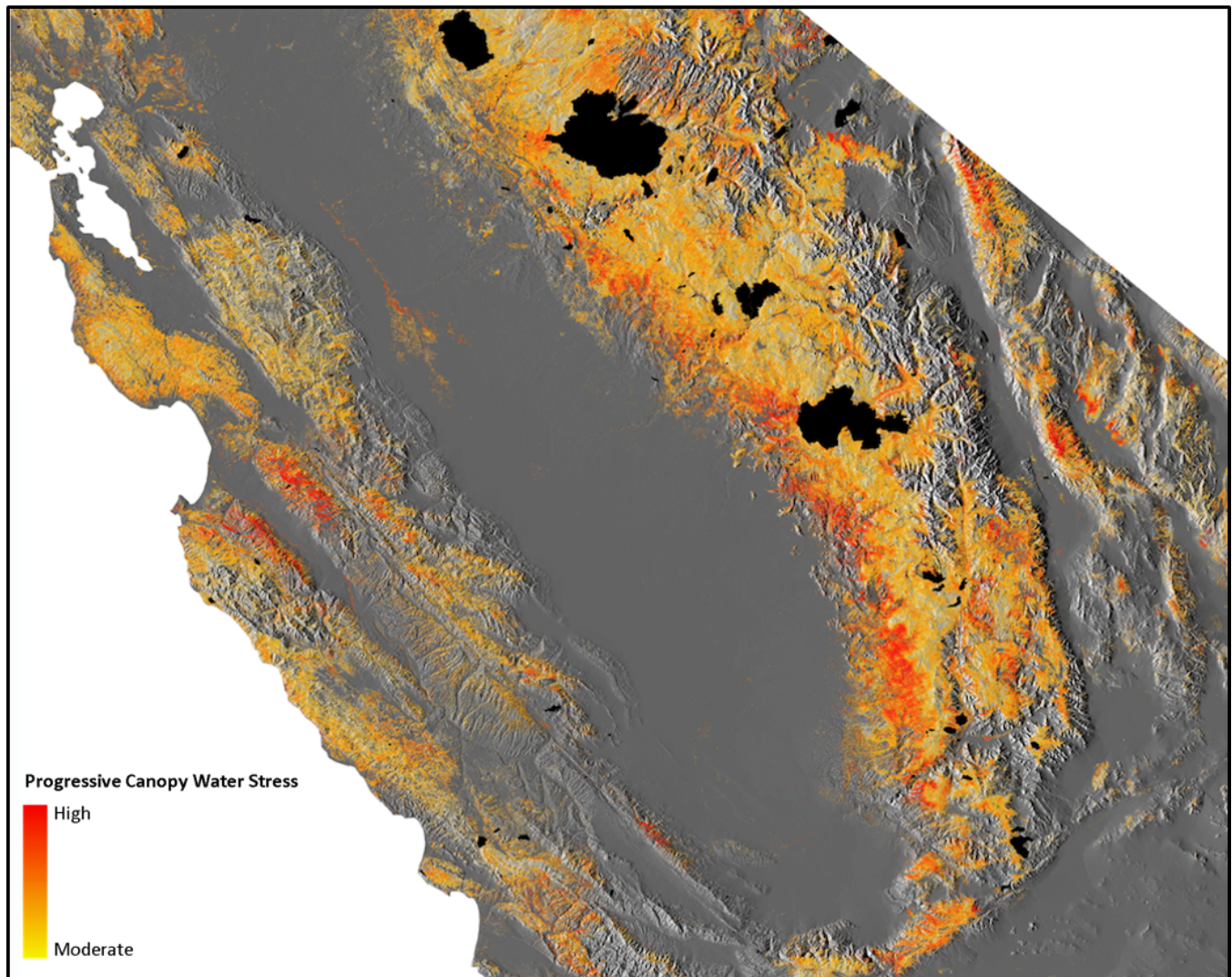


Fig. S16. Progressive forest canopy water stress for the years 2011 to 2015, computed as the sum of the percentage losses per observation period, for central California. Black areas indicate fire extents reported between 2011 and 2015 by the U.S. Forest Service. See Fig. 6 of the main text for the entire map of California.

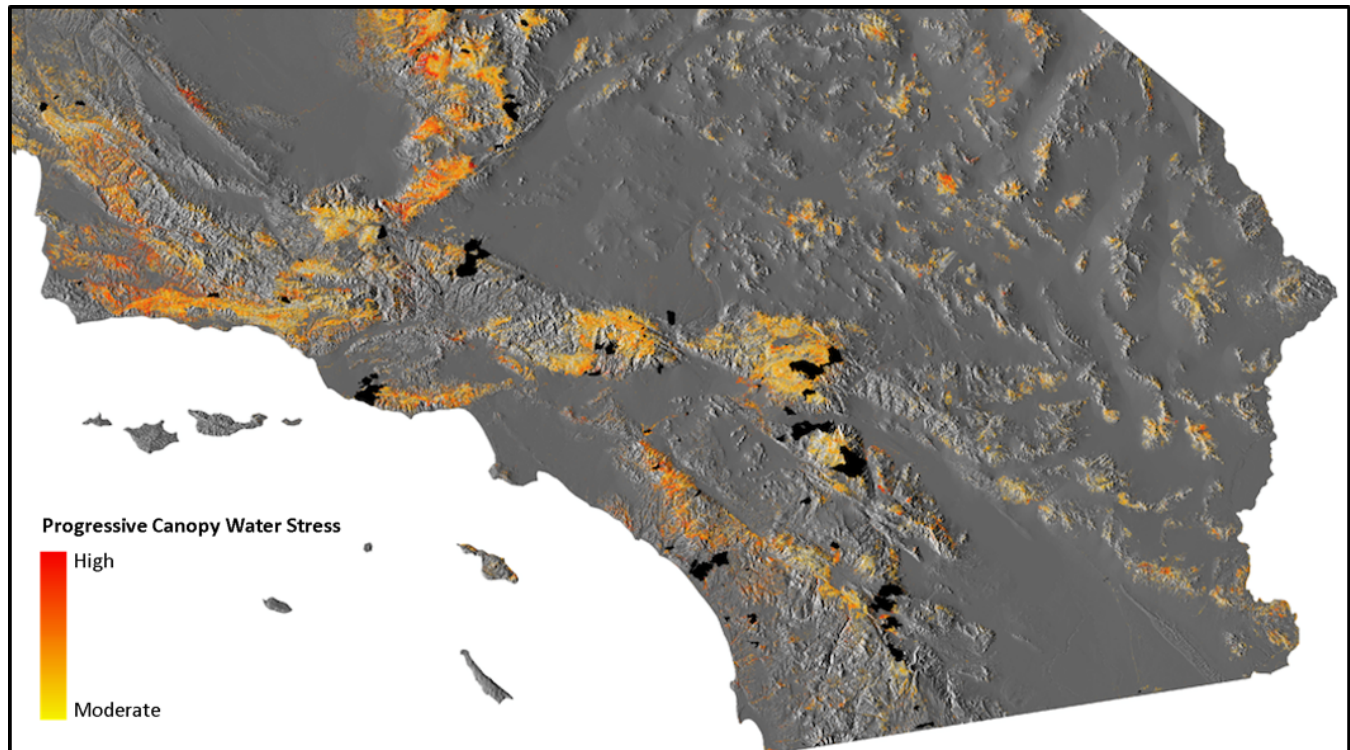


Fig. S17. Progressive forest canopy water stress for the years 2011 to 2015, computed as the sum of the percentage losses per observation period, for southern California. Black areas indicate fire extents reported between 2011 and 2015 by the U.S. Forest Service. See Fig. 6 of the main text for the entire map of California.